Exploring Synergy Between Tactile Perception and Arm Usage of Stroke Patients

A Pilot Study on Healthy Subjects

Yuhe Chen

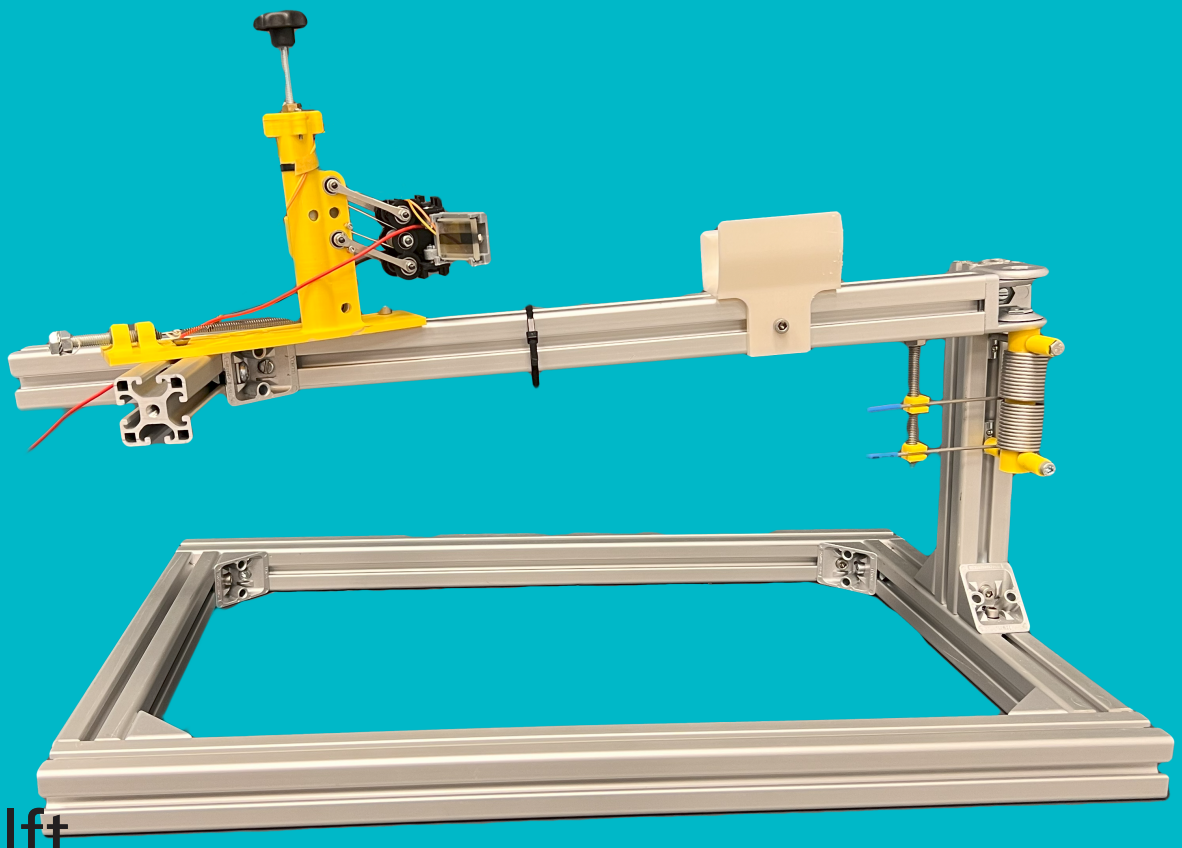

TU Delft

Exploring Synergy Between Tactile Perception and Arm Usage of Stroke Patients

A Pilot Study on Healthy Subjects

by

Yuhe Chen

in partial fulfilment of the requirements of:

Master of Science
in Biomedical Engineering
Track NeuroMusculoskeletal Biomechanics

at the Delft University of Technology,
to be defended publicly on Friday December 13, 2024 at 12:45 PM

Supervisor:	Arno Stienen	
Thesis committee:	Arno Stienen,	TU Delft, chair
	Jonathan van Zanten,	TU Delft
	Michaël Wiertlewski	TU Delft

An electronic version of this thesis is available at http://repository.tudelft.nl/.

TU Delft

Exploring Synergy Between Tactile Perception and Arm Usage of Stroke Patients: a Pilot Study on Healthy Subjects

Yuhe Chen

***Abstract*—Stroke causes severe tactile deficiencies, affecting motor control during object grasping and lifting. Understanding the fundamental neural disorders associated with tactile deficits is crucial for developing effective rehabilitation and treatment plans. Previous studies have investigated the dynamics between finger grasping behavior and arm muscle activation in stroke patients. However, the exact neuromuscular synergy between tactile perception and arm usage remains unexplored. In this study, we designed a comprehensive experimental platform and tested potential synergies in 12 healthy young adults, serving as a control group to establish a foundation for future studies on stroke patients. The experimental platform consists of a lever arm on which torques can be applied to the subject's arm. The end effector is equipped with a special ultrasonic friction modulation plate that can reduce apparent friction by up to 63%, simulating real-world grasping tasks in a controlled setting. The experiments were conducted under varying conditions of friction and arm usage. Results indicate significant effects of tactile stimulation on grasping force adaptation ($p < 0.05$ in 8 of 12 experimental conditions). In contrast, arm usage did not show significant synergy with tactile perception ($p = 0.44$ for grasping force adaptation amplitude, and $p = 0.73$ for reflex delay). These findings demonstrate that the experimental platform can provide insights into human tactile behaviors, which is critical for studying the synergy between tactile sensory and motor control. The results will lay the groundwork for future research on underlying pathologies and rehabilitation strategies for stroke patients.**

***Index Terms*—tactile perception, ultrasonic friction modulation, stroke, synergy**

I. Introduction

STROKE is the second-leading cause of death, and the third-leading cause of disability and death combined, as a study has revealed in 2021 [1]. More than 50% stroke patients reported perceptual disorders [2], including deficiencies in somatosensation [3] and proprioception [4]. These deficiencies cause stress, loss of daily task functions, and reduction of quality of life among stroke patients [5, 6]. Especially, impairment of tactile perception has a detrimental impact since patients have reported difficulty in sensing touch, pressure, and temperature, discriminating textures, and recognizing objects through tactile senses [7], as well as reduced or altered pain sensations [8]. To develop targeted treatment and rehabilitation strategies, it is crucial to understand the fundamental neural discrepancies associated with tactile deficits.

Tactile perception plays a fundamental role in manipulation tasks. Tasks as mundane as lifting and holding a cup or writing with a pen become tedious in the absence of touch. This issue is especially true when estimating the grasp force necessary to grasp an object securely [9]. Stroke patients may use abnormally high forces to ensure the security of grasping, and studies have suggested that during grasp-and-lift tasks, their grasping force fluctuates with the acceleration and deceleration of the object [10]. Accelerations and decelerations involve extensive activation of arm muscles, and the fluctuations of grasping force that occur at these moments are likely to be caused by tactile sensibility deficits [10]. Neuroscience research also brought evidence that brain damages caused by diseases like stroke induce impaired coordination of arm usage and grasp force prediction [11], and improper coupling of object grasping and lifting [12]. These correlations imply a possible neuromuscular synergy between tactile perception and arm muscle activation.

Despite increasing knowledge of the effect of friction on grasping [13], the effect of stroke on tactile functions or its effect on grasping is understudied [14]. Specifically, few studies have explored the dynamics of stroke patients' tactile perception deficits, and how they correlate with other neurological effects in complex tasks that involve the coordination of multiple neural inputs and outputs.

The absence of detailed knowledge of the impact of impaired touch on grasp is partially due to the difficulty of controlling tactile stimulation. Traditionally, changing tactile interaction is done by changing surface materials or using different gratings [15]. This method is tedious and it is often difficult to establish a general standard. But more importantly, it is impossible to study real-time responses to tactile stimulations.

However, a new class of haptic devices, called surface haptics, has emerged in recent years. These devices can modulate friction with the bare finger directly, either via electroadhesive effect or using ultrasonic vibration, see [16] for a comprehensive review. Contrary to electroadhesive devices, ultrasonic friction modulation can change the coefficient of friction on a wide dynamic range. It works by physically reducing the friction between the human finger and the surface [17] and the friction can be modulated from 1 all the way to near 0 [18]. The wide dynamics range makes it ideal for simulating real-world dynamics of grasping tasks.

The ultrasonic method was first introduced in 1995 [19]. Its functional mechanism to reduce friction involves the squeeze film effect in which ultrasonic waves create an overpressure between the finger and the vibrating plate. The air between the skin and the plate is squeezed into a thin film (Fig. 1), which slightly levitates the skin and reduces the number of asperities

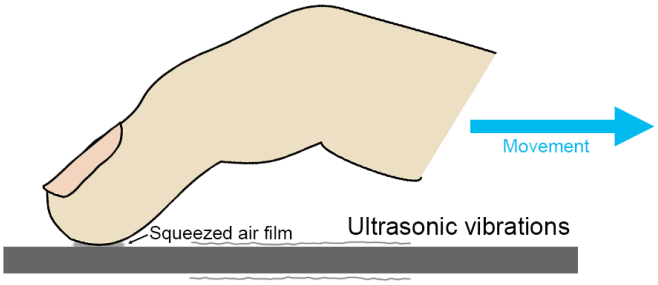

Fig. 1. Principle of ultrasonic friction modulation. The surface vibrates at an ultrasonic frequency, creating an air film between it and the finger, consequently lubricating the interface.

in contact, thus lowering friction [17, 18, 20].

We leverage ultrasonic friction modulation to study how human participants grasp objects. It is the first foray into understanding whether stroke patients suffering from neurological disorders have a synergy between arm usage and tactile perception. This paper serves as a pilot study, focusing on building the experiment platform and testing the hypothesis only on healthy subjects as a control group. The research question is: is there a synergy between human tactile perception and arm usage?

II. Materials and Methods

A. Goal

The goal of this experiment is to mimic a casual lifting task: a person grabs an object with a certain weight, lifts it to a certain height, with or without using arm muscles, and holds it for a certain time. The person does these all without special focus on the task itself to reflect real-life behaviors, whereas people also do not pay special attention when casually grasping objects. Specifically in this experiment, the friction level of the object is changed during a trial. The subject's grasping force and the object's angle are recorded and analyzed to evaluate the response to tactile stimulation.

B. Setup

The experiment setup (Fig. 2) can be broken down into four distinct sections: the grasping object (the black structure in Fig. 2a), the friction modulation plates (the glass plates in Fig. 2b), the constant force system (the yellow structure in Fig. 2c), and the elbow support (the aluminum extrusion profile structure in Fig. 2d). These sections each fulfill a specific need of this experiment. Appendix A elaborates on the design process and details of this setup.

1) Grasping Object: The grasping object (Fig. 3) mimics a general object to be grasped in everyday life. It also serves as a holder for the force sensors and the friction modulation plates. Two Futek LSB200 load cells are fixed on the object, while the friction modulation plate holders are connected to the object with one degree of movement freedom through a hinge-like structure. This structure unloads all irrelevant forces and torques, leaving only the grasping force to be exerted on the force sensors. The width of the object is 50 mm, and the

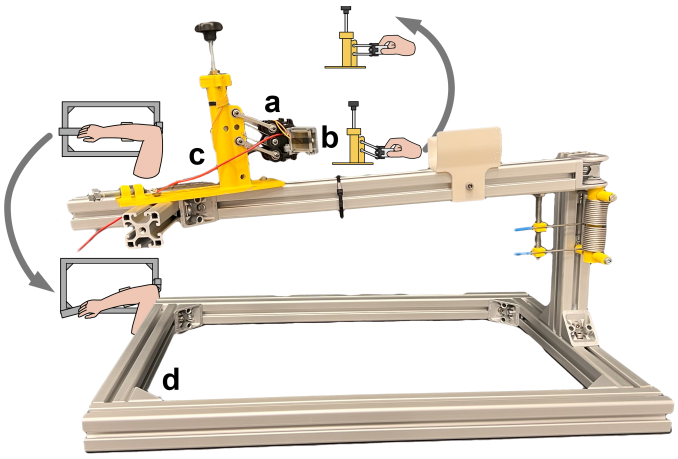

Fig. 2. Full assembly of the experimental setup. a) The grasping object. b) The friction modulation plates. c) The constant force system. d) The elbow support.

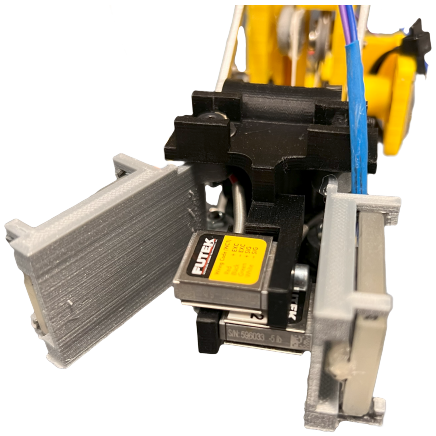

Fig. 3. Grasping object. The black structure is the base, which holds the silver square-shaped Futek LSB200 force sensors. The gray holders house the friction modulation plates.

effective grasping area is 34 × 25.5 mm. The base structure of the object was 3D printed with PLA, by an Ultimaker S5.

2) Friction Modulation Plates: Two friction modulation plates (Fig. 4) provide tactile stimulation on both sides of the grasping object. Each of them consists of a Steminc SMPL60W05T21F27R piezoelectric actuator (60 × 5 × 2.1 mm, cut to 34 mm lengthwise) glued on a borosilicate glass plate (34 × 25.5 × 5 mm) with 3M Scotch-Weld epoxy adhesive DP490. The setup uses digital function generators to generate two alternating voltage signals (sinusoidal, approximately 21 kHz, V_{pp} = 10 V), and amplified by voltage amplifiers to power the actuators. Details about the equipment can be found in Appendix A. When activated, the actuators vibrate the glass plates to an ultrasonic frequency (around 23 kHz), causing a 6.21 μm and a 5.72 μm displacement amplitude on the plates' centers respectively. Appendix A gives a full characterization of the ultrasonic vibration effect. This ultrasonic vibration provides the squeeze-film effect, greatly

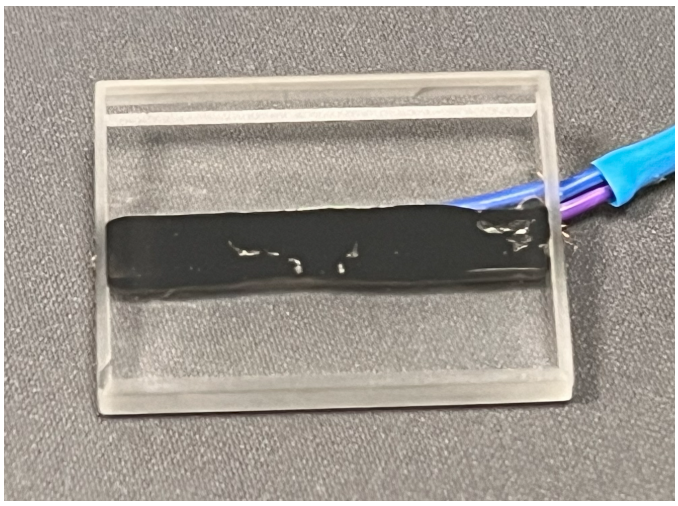

Fig. 4. One of the two friction modulation plates. A piezoelectric actuator was glued on the back of the glass plate with black epoxy glue. Two wires were soldered on the conductive layer on the actuator.

Fig. 5. Constant force system. The cylindrical structure houses a lead screw system, which adjusts the vertical force it provides. The screw at the lower-left corner connects to the pulley system and is used to adjust the pre-tension of the spring.

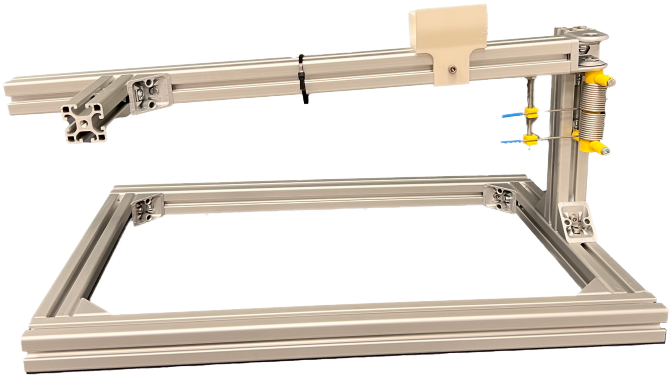

Fig. 6. Elbow support. The frame of the device is made of aluminum extrusion profiles. a) is a hinge. b) consists of a 3D-printed rod (yellow) and two torsion springs. c) is a 3D-printed wrist holder.

reducing the plates' surface friction. The specific amount of friction reduction is influenced by many factors and varies between subjects [21, 22]. From an empirical point of view, around 6 μm of vibration can result in a very satisfactory friction reduction effect (more than 80%) [21, 22]. The plates are squeeze-fitted into their holders on the grasping object. The holders each have four rubber-padded clamps, which secure the plates in place while providing sufficient damping.

3) Constant Force System: The constant force system (Fig. 5) provides an adjustable vertical force on the grasping object. This system consists of a pulley system and a parallel four-link mechanism connected to the object. The required force is provided by a Tevema T31115D extension spring within the pulley system. Details about this mechanism's principles and realizations are in Appendix A. This system is designed to provide a vertical force from - 5 N to + 5 N, adjusted by turning the black knob on the lead screw. The four-link limits the object's movement trajectory to a 50 mm radius circular arc. It is embedded with an AS5600 angular sensor, which measures the bars' angle. The base structure of the object was 3D printed with PLA, by an Ultimaker S5. The bars in the four-link were laser cut with 2 mm thick aluminum alloy plates.

4) Elbow Support: The elbow support (Fig. 2d) has a rotational stiffness. When the subject flexes their elbow to an angle, it can mimic the use of the arm in the object-grasping task. The subject rests their elbow on the hinge (Fig. 6a) and their wrist in the wrist holder (Fig. 6c). Two torsion springs (TV01740R, made by Tevema, 5.75 N·mm/degree) provide a clockwise (from the top view) torque on the horizontal arm-resting profile. At its neutral position, the profile's rotation is obstructed by the hinge and thus does not exert torque on the subject. During some trials, the subject is instructed to voluntarily flex their elbow to approximately 30 degrees, receiving approximately 4.14 N·m of torque. The base of the elbow support was built with aluminum extrusion profiles, while the wrist holder and the torsion spring housings were 3D printed with PLA, by an Ultimaker S5.

C. Controls and Data Acquisitions

A National Instruments USB-6008 terminal gathered force data from the load cells and angle data from the angular sensor via analog inputs. A Labview program reads the data at approximately 100 Hz. The data were then visualized in the program in real time and saved on the hard drive for analysis. The program runs on a ThinkPad T480s laptop.

The said Labview program also automatically executes every step of each trial. It controls the states of the friction modulation plates by sending a digital high/low signal to the external trigger of the function generators. The function generators are in the "Gated" mode, where they output the excitation signal when receiving a high voltage and vice versa. They use two separate channels to control the friction modulation plates.

D. Experiment Protocols

The main experiment studies three controlled variables: vertical force F_V on the object (-0.5, 0, 0.5 N), arm usage (yes, no), and friction perturbation (high to low, low to high). Among them, only the friction perturbation is program-controlled during a trial, while the two other variables are set prior to a trial. Thus a single trial has six (3×2) possible pre-defined combinations (Table I). To limit the experiment time for each participant, they were each given the task of 48 trials (12 familiarization trials + 36 actual trials). This left six trials for each pre-defined combination. The order of these combinations is randomized for each participant. A random friction perturbation is generated at the start of these six trials. This gives a uniform expected sample size of all 12 ($3 \times 2 \times 2$) controlled variable combinations, while the randomization eliminates possible bias introduced by any fixed trial order.

TABLE I
POSSIBLE PRE-DEFINED COMBINATIONS

Vertical Force (N)	Arm Usage
0.5	No
0.5	Yes
0	No
0	Yes
-0.5	No
-0.5	Yes

Before a trial, the constant force system is adjusted to the desired force level, and the subject is asked to relax or flex their elbow. Note that when the force on the object is 0 N, there is no actual need to change the grasping force when there is a change in friction. So this group acts as a "placebo" control to account for factors like vibration, heat, and habitual behavior, excluding the effects of friction change on the results.

The participant task includes three program-controlled phases:

1) Lifting phase. This phase has no time limit. The initial friction state is applied before the start of this phase. During this phase, the subject is asked to lift the object to approximately horizontal with an optimal grasp effort. The optimal effort means applying the minimal grasping force necessary while ensuring grasp stability. The protocol automatically proceeds to the next phase when 1) the object's average angle position displacement is greater than 10 degrees, 2) the standard deviation of the lifted angle is below 0.75 degrees, and 3) the standard deviation of the grasping force is below 0.075 N. These metrics are calculated using data from the last 0.5 seconds.
2) Holding phase 1. This phase lasts for 2 seconds. It is used to establish a steady baseline of the initial grasping force. Data from the beginning of this phase are used for further analysis.
3) Holding phase 2. This phase lasts for 8 seconds. Immediately at the start of this phase, the friction state switches to the opposite as a perturbation. The subject's goal is to maintain the object's position.

After the trial, the friction modulation will be turned off, and the subject can let go of the object. Fig. 7 summarizes the entire protocol and different controlled variables. Fig. 8 depicts a typical trial. The subject is currently holding the object while watching the nature documentary.

During the experiment, the subject is asked to wear a pair of Sony WH-1000XM4 active noise-canceling headphones to avoid any audio cues. In the meantime, a documentary *Our Planet* Season 2 Episode 2 is played to them to divert their attention, to mimic a casual grasping task. The subject is told that they will fill in a simple quiz (Appendix C) related to the documentary after the experiment is finished. The subject is asked to take a break every 10 minutes to avoid muscle fatigue and to let the equipment cool down. The whole experiment takes approximately 50 minutes for each subject.

E. Friction Modulation Characterization

Before the main experiment, subjects were asked to perform a qualitative test to characterize the effectiveness of friction reduction. The object was adjusted to have a force of 0.5 N downwards. The subject would first squeeze the object with excessive force and lift it. Then, they would gradually reduce their grasping force until the object started to slip slowly. They were instructed to continue to release their grip until the object fully slipped from their fingers. They repeated this process with friction reduction either off (high friction) or on (low friction). Their grasping force and the object's position during the whole process were recorded and analyzed. Assuming a simple friction model, the minimum grasping force before the object slips provides a friction force equal to the object's vertical force.

F. Data Processing

1) Data Cleaning: Grasping force and object angle data were cleaned before further analysis. First, their zero baselines were subtracted. The force's baseline was determined by two steps:

1) The computer reads the force data after an analog-digital converter, so the recorded force data is discrete. An initial baseline takes the most frequent value in the data array, assuming that when any force is applied to the force sensors, it would not be stable enough to have a greater number than when there is no force.
2) A more precise baseline was determined by using the initial value plus 0.01 N as a threshold and taking the average of all values under this threshold.

The angle data do not need a precise zero baseline, so the baseline was simply determined by the lowest value of the data array.

Next, data were segmented into trials and stored in separate arrays. The data acquisition rate was set to be 100 Hz; however, due to hardware limitations, the actual sampling was approximately 65 Hz, with a variable sampling rate. So, all segments were resampled to 100 Hz with a polyphase antialiasing filter.

2) Data Exclusion: A threshold was used for detecting human errors in the trials (see Appendix B). The value was determined by 10 times the minimum grasping force needed

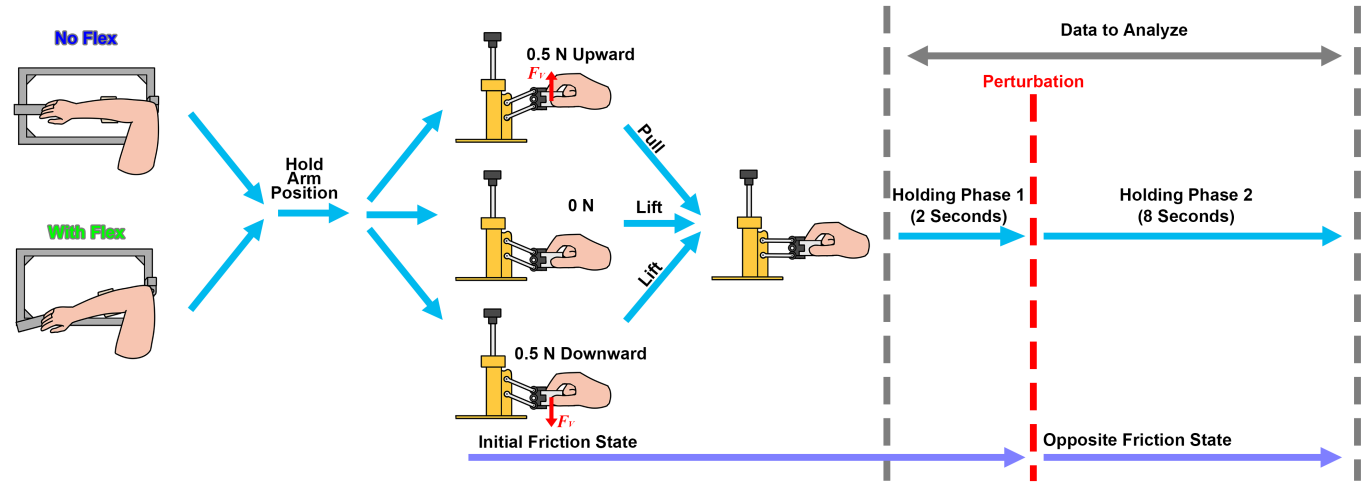

Fig. 7. Flowchart of the experimental protocol. Controlled variables are 1) Elbow position (no flex, with flex; illustrated by the elbow drawings on the left), the subject keeps their elbow position during the entirety of the trial; 2) Vertical force F_V (0.5 N upward, 0 N, 0.5 N downward, illustrated by the hand drawings in the middle), the trial data used is the 10 seconds after they have lifted/pulled the object and stabilized; 3) Friction perturbation (high to low, low to high; shown by the purple arrows on the bottom), the initial friction state starts before the subject touches the object.

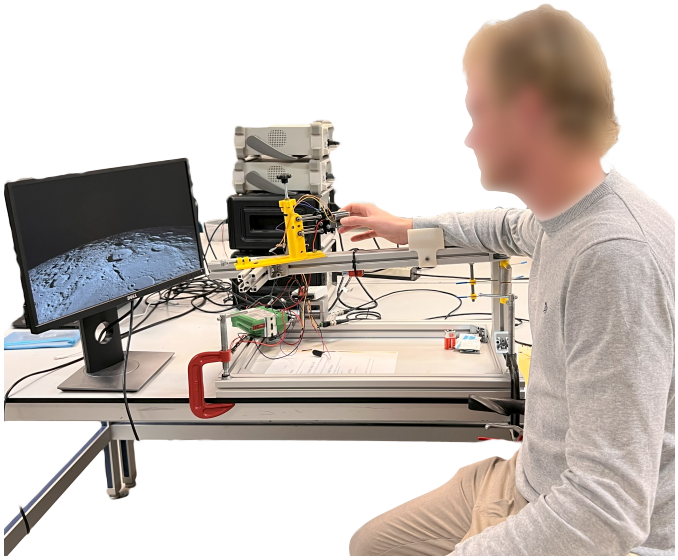

Fig. 8. A typical scene where a participant is performing the experiment. They are currently in the holding phase of a trial, not flexing their elbow, while watching the nature documentary.

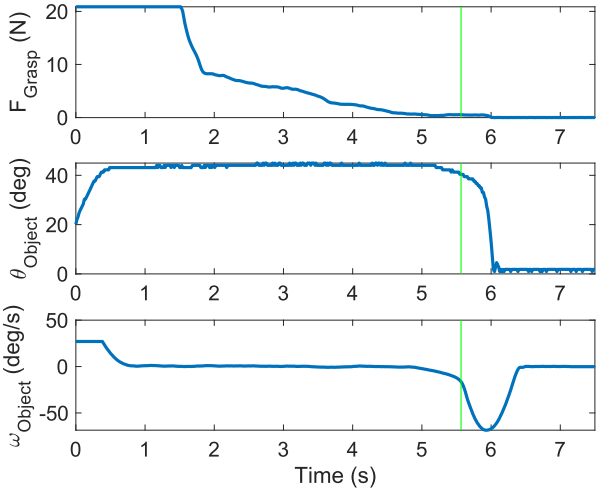

Fig. 9. A typical friction modulation characterization test. The graphs from top to bottom represent the grasping force F_{Grasp}, the object's angle θ_{Object}, and its derived angular velocity ω_{Object}, over time. The green vertical line indicates the program-detected start-to-slip point.

at the low friction condition (8.56 N in this case, as will be later shown in the results section). Further analysis excludes all trials with force exceeding this threshold. 12 trials were excluded in total among 432 trials.

3) Characterization Data: Fig. 9 shows a typical characterization test. The object's angular velocity ω_{object} is the time derivative of its angle θ_{object}, with a moving window average of 50 samples (across 0.5 s) to eliminate analog-digital conversion artifacts. Then, the most significant change point in the angular velocity's root mean square (green lines in Fig. 9) determines when the object starts to slip. It is assumed that the object first slips in a uniform motion, and the friction force is equal to its vertical force (0.5 N) at this point. The minimum grasping force before this point represents the minimum grasping force required to achieve such a level of friction.

4) Metric Extraction: Fig. 10 shows a typical trial where the friction changes from high to low on the two-second point (red lines), and the object has a downward vertical force. The upper plot is the grasping force F_{Grasp}, while the lower one is the object's position θ_{Object}. The object's position does not significantly change during a trial and is not in the scope of this experiment, thus it is not further studied.

Three metrics were extracted from each trial: the initial grasping force before the perturbation $F_{initial}$, the end force after full adaptation F_{end} (the cyan and magenta lines in Fig. 10), and the difference between them ΔF_{end}. They are calculated by:

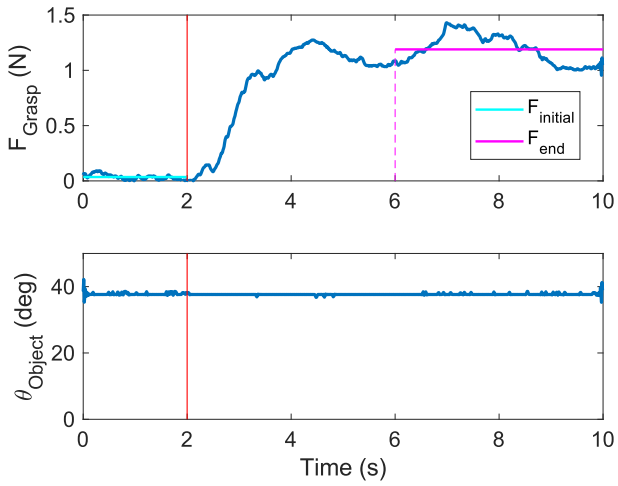

Fig. 10. A typical trial where the friction changes from high to low, and the object has a downward vertical force. The upper plot shows the grasping force F_{Grasp} over time, and the lower one shows the object's angle θ_{Object} over time. The vertical red lines indicate the time of the friction change (2 s). The horizontal magenta lines show the initial force before the perturbation and the end force after the perturbation.

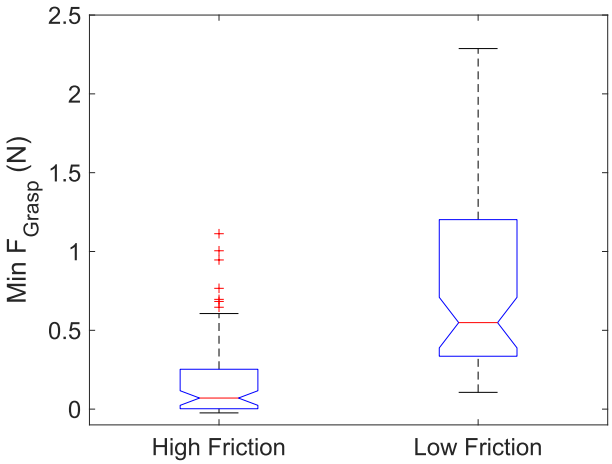

Fig. 11. Effect of friction modulation. The boxes represent the minimum grasping force $min(F_{Grasp})$ required to generate 0.5 N of tangential friction under different conditions (N = 72 for both conditions). The high friction condition has nine outliers; while the low friction condition has two outliers.

$$\begin{cases} F_{initial} = mean(F_{Grasp}(t < 2)) \\ F_{end} = mean(F_{Grasp}(t > 6)) \\ \Delta F_{end} = F_{end} - F_{mean} \end{cases} \quad (1)$$

The reason F_{end} is not calculated directly after the perturbation is that the adaptation for grasping forces takes time, especially in friction-increasing conditions (which will be shown in the next section). So, the calculation uses the second half of the data (from 6 s to 10 s) after the perturbation.

G. Adaptations from Earlier Research

This experiment also adapted several suggestions from an earlier similar study [23]. Per their recommendations, this experiment did not give a cue to subjects when their grasping force was too high but rather relied on their natural instinct to optimize their force. Also, to avoid finger sweating affecting the friction, subjects were instructed to thoroughly wash their hands with soap immediately before the experiment and were provided alcohol swipes to clean their fingers anytime during the experiments.

H. Participants

This experiment recruited 12 participants, including seven males and five females. They are all healthy adults with no diagnosed tactile or arm usage deficiencies. Their age ranges from 24 to 30 (mean 26.4). Since the experiment setup is specifically designed for right-hand use, only right-handed individuals were recruited.

III. Results

A. Friction Modulation Effect

Fig. 11 shows the statistics of the minimum grasping force. A paired t-test for the mean values of each subject further confirmed that the friction reduction has a significant effect on the grasping force ($t_{12} = -3.3, p = 0.0069$).

The average minimum force for the high friction condition is 0.32 N, while that of the low friction condition is 0.86 N. Assuming a simple friction model without viscosity, the ultrasonic friction effectively reduced the surface friction coefficient by 63%. Note that the actual friction model is more complex and depends on the subject [21], so this value is just for qualitative reference.

B. Data Overview

Fig. 12 plots the force data of all 12 conditions separately. The blue lines indicate when the subject does not flex their elbow, while the green lines indicate the opposite. Shaded areas are their standard deviations. The left column indicates when the friction changes from low to high, while the right one indicates otherwise. The rows from top to bottom indicate 0.5 N upward, 0 N, and 0.5 N downward vertical force on the object, respectively. Fig. 13 further illustrates the mean and standard deviations of the difference in grasping force ΔF_{Grasp} over time. ΔF_{Grasp} has a similar definition as ΔF_{end}:

$$\Delta F_{Grasp}(t) = F_{Grasp}(t) - F_{initial} \quad (2)$$

Note that here the mean was taken from all trials, not from each subject's mean data.

IV. Discussions

A. Experiment Validation

Before addressing the primary research question, it is essential to establish the validity of the experiment. The validation entails demonstrating that the results accurately reflect the participants' tactile perception and align with established findings in the field. Fig. 14 shows the confidence levels ($1-p$) of paired t-tests ($N = 12$) between $\overline{F}_{initial}$ and $\overline{F}_{end}$ of each

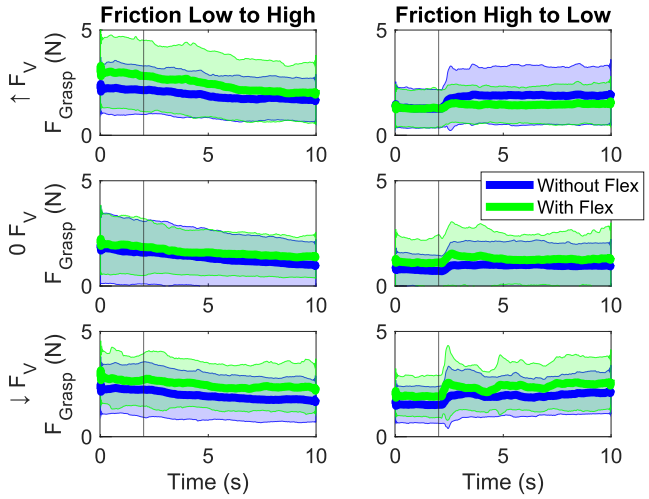

Fig. 12. Overview of $\overline{F}_{Grasp}$ over time under 12 different conditions. The blue lines indicate when the subject does not flex their elbow, while the green lines indicate otherwise. Shaded areas are their standard deviations. The left column indicates when the friction changes from low to high, while the right one indicates otherwise. The rows from top to bottom indicate 0.5 N upward, 0 N, and 0.5 N downward vertical force F_V on the object respectively.

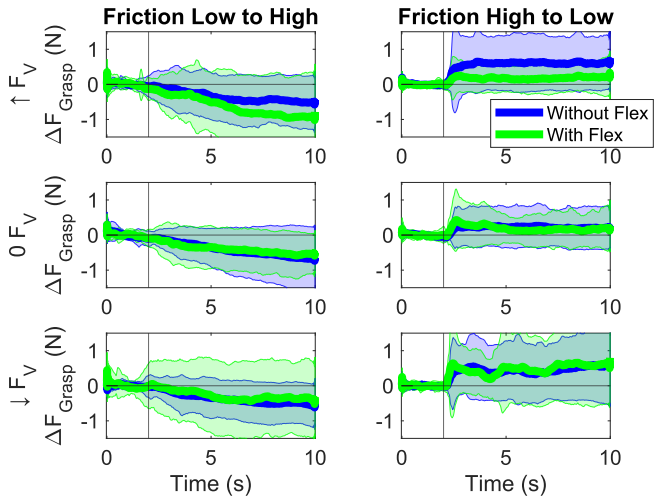

Fig. 13. Overview of the mean of $\Delta\overline{F}_{Grasp}$ over time under 12 different conditions. ΔF_{Grasp} is the force data F_{Grasp} subtracted by $F_{initial}$. The blue lines indicate when the subject does not flex their elbow, while the green lines indicate otherwise. Shaded areas are their standard deviations. The left column indicates when the friction changes from low to high, while the right one indicates otherwise. The rows from top to bottom indicate 0.5 N upward, 0 N, and 0.5 N downward vertical force F_V on the object respectively.

subject under different conditions. Since the confidence levels are all above 85% and 8 out of 12 are above 95%, it is a clear indication that the friction perturbation has a significant impact on the participants' ability to regulate their grasping force.

Furthermore, there is no statistical difference when it comes to the direction of the vertical force ($t_{24} = -1.1, p = 0.3$, and $t_{24} = -0.96, p = 0.34$ for friction increasing and decreasing, respectively). Thus, the upward force and downward force groups can be combined as "with vertical force" experimental groups, with respect to "no vertical force" control groups.

However, it seems that the "control" groups (no vertical

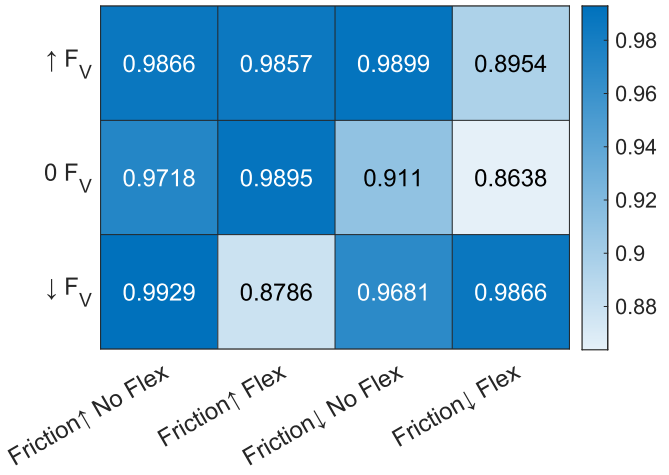

Fig. 14. Heatmap of confidence levels of paired t-tests between $\overline{F}_{initial}$ and $\overline{F}_{end}$ (as in Fig. 10) of each subject under different variable combinations (arm usage, vertical force F_V direction, friction change). The higher the value, the deeper the color, and the more significant that the perturbation had an effect.

force but with friction perturbation) also demonstrated a significant effect of tactile stimulation on the grasping behaviors. So, paired t-tests of $\Delta\overline{F}_{end}$ comparing trials with and without a vertical force are performed. In these tests, all other conditions are combined except for the friction perturbation because it affects the positivity of force adaptation. Results showed that there is no significant difference between the no vertical force "control" groups and the experiment groups when friction increases ($t_{24} = 1.1, p = 0.3$). In contrast, when the friction decreases, the experiment groups exhibit significantly greater force adaptation ($t_{24} = -2.9, p = 0.0088$). This significance confirms that in decreasing friction conditions, participants can actually perceive and adapt to friction change, rather than habitually responding to irrelevant factors such as heat or vibration.

Taking all factors into account, it is clear that the subjects can perceive the change in friction and adapt accordingly, with the current experiment setup and protocol. Thus, this experiment reflects their tactile perceptions.

B. General Grasping Behavior

1) Decreasing Friction: Subjects increase their grasping force when the friction decreases and they sense an actual need to grasp tighter. Their reactions can resemble a first-order system, where there is a small delay after the impulse (perturbation), and then the system output (grasping force) increases negative exponentially to a new steady state, as the lines on the right side of Fig. 13 suggest. In fact, the delay t_{delay} can be calculated if fitting the force curve with a piecewise function after the perturbation:

$$\begin{cases} \Delta\hat{F}(t < t_{delay}) = 0 \\ \Delta\hat{F}(t \geq t_{delay}) = A \times (1 - e^{\frac{-(t-t_{delay})}{\tau}}) \end{cases} \quad (3)$$

Where A is the gain and τ is the time constant. Because individual trials often have very large deviations, the goodness

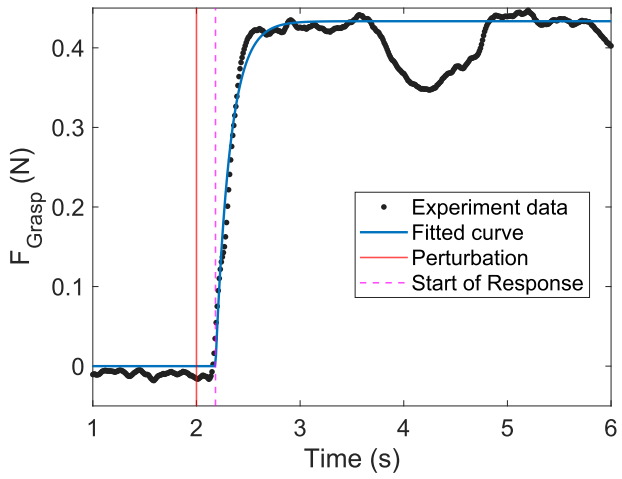

Fig. 15. Fitted curve of the grasping force F_{Grasp}. It takes the mean of all trials with decreasing friction and non-zero vertical force. The black dots represent the experiment data points, while the blue line is the fitted curve. The red vertical line marks the start of the perturbation. The fitted time delay of the system is 184 ms, which is marked by the dashed magenta line.

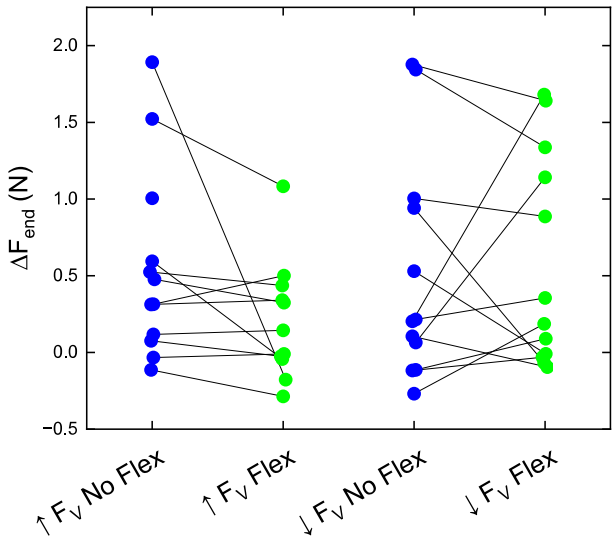

Fig. 16. Comparison of each subject's ΔF_{end} with and without arm usage. The left part of the figure is when the vertical force F_V is set upward, and the right part is when the vertical force is set downward. Blue dots are without arm usage, and green dots are with arm usage. Note on the left side there is an abnormally huge decrease in one of the participants.

of fit is not always satisfactory. As a consequence, only the average of every trial with decreasing friction and non-zero vertical force was fitted with the non-linear least squares method, as shown in Fig. 15. The resulting time delay is 184 ms. The delay is slightly larger than previous findings on friction-induced reflex response time [24], but still in the same magnitude. It is also consistent with the previous study [23]. This short delay implies that there is an intrinsic reflex pathway in humans to react to sudden grasp instability.

2) Increasing Friction: A decrease in grasping force is observed when the friction increases during a trial, at a significantly slower rate than when friction decreases (Fig. 13). However, the "control" groups (where there is no actual need to change the grasping force) showed a similar level of grasping force decrease as the experimental groups. This similarity suggests that the decrease in grasping force might be caused by factors other than friction change. When comparing the increasing and decreasing friction conditions, the amplitude of the grasping force change ΔF_{end} does not show a significant difference ($t_{72} = 1.35, p = 0.18$). It means they adapt to the same level of friction change, no matter the positivity, with the same level of grasping force change. Taking this factor into consideration, the grasping behavior in the increasing friction condition might fall into these hypotheses:

1) The actual grasping force is a lot higher than the minimum required grasping force, even in low friction conditions (see Fig. 12 and Fig. 11). Therefore, the decrease in the grasping force is merely an attempt to optimize the grasping force, and the subject does not perceive the decrease in friction.
2) Since there is no actual grasping force needed in the no vertical force group, the subjects also felt the need to reduce their grasping force, as the same in situations where friction increases. However, the amplitude of this reduction in grasping force happens to coincide with that in non-zero vertical force conditions. Thus, although the subject can perceive the friction increase, the results yield no statistical difference.

This observation is different from the previous study [23], as they reported no significant decrease in grasping force with increasing friction. Since this experiment lacks the data or motive to support either hypothesis, this finding is not further explored.

C. Effects of Arm Usage

1) Effects on Grasping Force: Fig. 12 suggests that there is a difference between the grasping force with and without arm usage, regardless of the perturbation. The no vertical force groups were not taken into account. A paired t-test between each subject's $\overline{F}_{initial}$ without and with arm usage under all other conditions confirmed there is a significant effect of arm usage on the magnitude of the grasping force ($t_{48} = -3.8, p = 4.2 \times 10^{-4}$). The same test on their $\overline{F}_{end}$ yields similar results ($t_{48} = -3, p = 0.0039$), suggesting that when participants are using their arms, they use a significantly higher grasping force both at the beginning of the grasping task and at the steady state where they have adapted to the new friction level.

2) Effects on Force Change: Since it is not confirmed that the friction-increase conditions reflect tactile perception, only friction-decrease conditions are considered in this evaluation. A paired t-test between each subject's $\Delta\overline{F}_{end}$ without and with arm usage proved no significant difference ($t_{24} = 0.79, p = 0.44$). The subjects adapt to the same level of friction change with the same amplitude of force change, regardless of the usage of their arm. Although there seems to be a large difference on the upper right plot of Fig. 13, it was actually caused by a single participant's abnormal data (see Fig. 16). The principles of the paired t-test here rule out this discrepancy.

3) Effects on Time Delay: Using 3, response delay t_{delay} can be calculated for every subject under decreasing friction. However, due to the high deviations of each trial, this function was only successfully fitted to 8 subjects with meaningful results. A paired t-test between these subjects' t_{delay} without and with arm usage proved no significant difference ($t_8 = -0.35, p = 0.73$). This result suggests that arm usage does not affect the time delay of response to tactile perception.

4) Is There a Synergy?: In conclusion, subjects consistently applied greater grasping force when using their arms, regardless of the condition. However, several participants reported unintentionally using their hands to assist in bending the elbow support (refer to the mechanism in Fig. 2). Despite this, they demonstrated similar responses to tactile perturbations, maintaining the same amplitude of force adaptation and likely the same level of time delay. The participants' feedback, combined with the unchanged amplitude of force adaptation regardless of arm usage, suggest that the increased grasping force is likely due to additional hand pressure on the plates. Taking all factors into account, it can be concluded that in healthy young adults, there is no significant neuromuscular synergy between arm usage and tactile perception.

V. Reflections

A. Experiment Setup

1) Friction Plates: The ultrasonic friction plates are remarkable tools for exploring questions related to human tactile perception. However, because they rely on ultrasonic vibration, the force applied to them dampens the amplitude, which might affect friction. This results in a non-linear relationship between the grasping force and the friction. Furthermore, the required grasping force cannot be too high, so subsequently, the vertical force on the object cannot be too high. Lower forces then bring a lower signal-to-noise ratio. A possible solution to this is to use more actuators, thus having more power to counter the grasping pressure, but this still does not completely fix the damping problem and will result in a bulkier setup.

2) Constant Force System: The constant force system does provide a smoother action than any motorized system could match. Although the calculations and design of the constant force system's structure were thorough and precise, its actual performance was not as stable as expected. The measuring of its output force somehow varies with time. Although the variance is small (< 1 N), it still resulted in the output vertical force not exactly being 0.5 N. This might be due to the high tolerances of 3D-printed parts. Switching to higher precision printing techniques or CNC machining may solve the problem.

3) Elbow Support: The elbow support was improvised, thus not addressing all aspects of functionalities. For example, 1) the device can only be used on right-handed people, 2) the torque on the device is not properly characterized and is not adjustable, and 3) the subjects might involuntarily use their hand to assist in elbow bending, which was discussed earlier. It may be necessary for further studies to iterate this device with these shortcomings in mind.

B. Experiment Methods

1) Adaptations From the Previous Study: This experiment took some advice from another similar research [23] and yielded good results. Firstly, most participants loved the idea of watching the nature documentary. They reported that the documentary effectively diverted their attention from the task itself during the trial. This allowed recordings of more natural and intuitive responses, reducing human psychological factors. Furthermore, they all agreed that the documentary made the experiment more enjoyable. Secondly, not giving "force-too-high" audio cues to participants did not affect their grasping strategy. They all learned the optimal grasping force fairly quickly and well within the 12 familiarization trials. These practices are recommended for similar research in the future.

2) Participants: This experiment strives to achieve equality in sexes when recruiting participants to avoid gender bias and succeeded with a combination of 5 females and 7 males. However, the sample size was relatively small due to time constraints. Although the power of this experiment was sufficient for its major findings, more samples may help to reveal deeper issues, like the time delay problem. Also, since all the subjects reported the experiment to be enjoyable, it is possible to prolong the experiments for more samples.

3) Vertical Force Direction: Since it is already proven that the direction of the vertical force has no significant impact on subjects' grasping response, a single direction should be sufficient for future research.

VI. Conclusions

We presented a pilot study involving healthy subjects that explores if there is a neuromuscular synergy between stroke patients' arm usage and their tactile perception of the object in hand. To achieve this, we built an experiment setup that can both induce arm usage and provide tactile perturbation to subjects by reducing or increasing friction. The results revealed a general grasping behavior that is consistent with earlier findings, which confirmed that this experiment is valid in revealing possible tactile perception discrepancies. In the end, we found that there is no significant evidence that arm usage has a synergy with healthy subjects' tactile perception. This conclusion hints at the fact that for healthy humans, the regulation of grasp might be an independent process of general motor control.

VII. Acknowledgments

I give my sincere thanks to my supervisor Professor Arno Stienen and my daily supervisor Jonathan van Zanten and all their jokes. They have been more supportive and attentive throughout the entirety of my graduation project than I could have ever asked for. Thanks to Professor Michaël Wiertlewski and Zhaochong Zhang for their time and enormous help with the haptic part of this project. Thanks to Jan van Frankenhuyzen for the valuable engineering support and insightful talks. Thanks to Sinclair who helped me draw the nice icons. Thanks to all the lovely victims who have sacrificed their time to participate in my research. Thanks to all the supportive staff at workshops who have helped me with my project. Also

thanks to everyone at Arno's group and down at the basement for your professional help and company. Last but not least, thanks to my family and friends who may not be here but supported me spiritually. I could not express enough gratitude to everyone on my journey here at TU Delft.

REFERENCES

[1] V. L. Feigin *et al.*, "Global, regional, and national burden of stroke and its risk factors, 1990–2019: A systematic analysis for the Global Burden of Disease Study 2019," *The Lancet Neurology*, vol. 20, no. 10, pp. 795–820, Oct. 1, 2021, ISSN: 1474-4422. DOI: 10.1016/S1474-4422(21)00252-0. [Online]. Available: https://www.sciencedirect.com/science/article/pii/S1474442221002520.

[2] L. M. Carey and T. A. Matyas, "Frequency of discriminative sensory loss in the hand after stroke in a rehabilitation setting," *Journal of Rehabilitation Medicine*, vol. 43, no. 3, pp. 257–263, Feb. 2011, ISSN: 1651-2081. DOI: 10.2340/16501977-0662. pmid: 21305243.

[3] S. S. Kessner, U. Bingel, and G. Thomalla, "Somatosensory deficits after stroke: A scoping review," *Topics in Stroke Rehabilitation*, vol. 23, no. 2, pp. 136–146, Feb. 17, 2016, ISSN: 1074-9357. DOI: 10.1080/10749357.2015.1116822. [Online]. Available: https://doi.org/10.1080/10749357.2015.1116822.

[4] J. E. Aman, N. Elangovan, I.-L. Yeh, and J. Konczak, "The effectiveness of proprioceptive training for improving motor function: A systematic review," *Frontiers in Human Neuroscience*, vol. 8, Jan. 28, 2015, ISSN: 1662-5161. DOI: 10.3389/fnhum.2014.01075. [Online]. Available: https://www.frontiersin.org/journals/human-neuroscience/articles/10.3389/fnhum.2014.01075/full (visited on 09/03/2024).

[5] C. Hazelton *et al.*, "Interventions for perceptual disorders following stroke - Hazelton, C - 2022 — Cochrane Library," ISSN: 1465-1858. [Online]. Available: https://www.cochranelibrary.com/cdsr/doi/10.1002/14651858.CD007039.pub3/full (visited on 09/03/2024).

[6] J. E. Sullivan and L. D. Hedman, "Sensory dysfunction following stroke: Incidence, significance, examination, and intervention," *Topics in Stroke Rehabilitation*, vol. 15, no. 3, pp. 200–217, May 1, 2008, ISSN: 1074-9357. DOI: 10.1310/tsr1503-200. pmid: 18647725. [Online]. Available: https://doi.org/10.1310/tsr1503-200 (visited on 09/03/2024).

[7] L. M. Carey, "Somatosensory loss after stroke," *Critical Reviews™ in Physical and Rehabilitation Medicine*, vol. 7, no. 1, 1995, ISSN: 0896-2960, 2162-6553. DOI: 10.1615/CritRevPhysRehabilMed.v7.i1.40. [Online]. Available: https://www.dl.begellhouse.com/journals/757fcb0219d89390,58e9038f7231b7dc,7af41ca30975d27f.html (visited on 09/03/2024).

[8] H. Klit, N. B. Finnerup, G. Andersen, and T. S. Jensen, "Central poststroke pain: A population-based study," *Pain*, vol. 152, no. 4, p. 818, Apr. 2011, ISSN: 0304-3959. DOI: 10.1016/j.pain.2010.12.030. [Online]. Available: https://journals.lww.com/pain/abstract/2011/04000/central_poststroke_pain__a_population_based_study.19.aspx (visited on 09/03/2024).

[9] R. S. Johansson and G. Westling, "Roles of glabrous skin receptors and sensorimotor memory in automatic control of precision grip when lifting rougher or more slippery objects," *Experimental Brain Research*, vol. 56, no. 3, pp. 550–564, Oct. 1, 1984, ISSN: 1432-1106. DOI: 10.1007/BF00237997. [Online]. Available: https://doi.org/10.1007/BF00237997 (visited on 09/03/2024).

[10] J. Hermsdörfer, E. Hagl, D. Nowak, and C. Marquardt, "Grip force control during object manipulation in cerebral stroke," *Clinical Neurophysiology*, vol. 114, no. 5, pp. 915–929, May 1, 2003, ISSN: 1388-2457. DOI: 10.1016/S1388-2457(03)00042-7. [Online]. Available: https://www.sciencedirect.com/science/article/pii/S1388245703000427.

[11] D. A. Nowak and J. Hermsdörfer, "Objective evaluation of manual performance deficits in neurological movement disorders," *Brain Research Reviews*, vol. 51, no. 1, pp. 108–124, Jun. 1, 2006, ISSN: 0165-0173. DOI: 10.1016/j.brainresrev.2005.10.003. [Online]. Available: https://www.sciencedirect.com/science/article/pii/S0165017305001347.

[12] M. Davare, M. Andres, G. Cosnard, J.-L. Thonnard, and E. Olivier, "Dissociating the Role of Ventral and Dorsal Premotor Cortex in Precision Grasping," *The Journal of Neuroscience*, vol. 26, no. 8, p. 2260, Feb. 22, 2006. DOI: 10.1523/JNEUROSCI.3386-05.2006. [Online]. Available: http://www.jneurosci.org/content/26/8/2260.abstract.

[13] L. Willemet, F. Roël, D. Abbink, I. Birznieks, and M. Wiertlewski, "Grip force control under sudden change of friction," *Journal of Physiology*, in press.

[14] D. A. Nowak and J. Hermsdörfer, "Grip force behavior during object manipulation in neurological disorders: Toward an objective evaluation of manual performance deficits," *Movement Disorders*, vol. 20, no. 1, pp. 11–25, 2005, ISSN: 1531-8257. DOI: 10.1002/mds.20299. [Online]. Available: https://onlinelibrary.wiley.com/doi/abs/10.1002/mds.20299 (visited on 09/03/2024).

[15] R. S. Johansson, "Sensory input and control of grip," in *Sensory Guidance of Movement*, G. R. Bock and J. A. Goode, Eds., vol. 218, 1998, pp. 45–63, ISBN: 1528-2511.

[16] C. Basdogan, F. Giraud, V. Levesque, and S. Choi, "A review of surface haptics: Enabling tactile effects on touch surfaces," *IEEE Transactions on Haptics*, vol. 13, no. 3, pp. 450–470, Jul. 2020, ISSN: 1939-1412. DOI: 10.1109/TOH.2020.2990712.

[17] M. Biet, F. Giraud, and B. Lemaire-Semail, "Squeeze film effect for the design of an ultrasonic tactile plate," *IEEE Transactions on Ultrasonics Ferroelectrics and Frequency Control*, vol. 54, no. 12, pp. 2678–2688, Dec. 2007, ISSN: 0885-3010. DOI: 10.1109/TUFFC.2007.596.

[18] M. Wiertlewski, R. F. Friesen, and J. E. Colgate, "Partial squeeze film levitation modulates fingertip friction," *Proceedings of the National Academy of Sciences of the United States of America*, vol. 113, no. 33, pp. 9210–9215, Aug. 16, 2016, ISSN: 0027-8424. DOI: 10.1073/pnas.1603908113.

[19] T. Watanabe and S. Fukui, "A method for controlling tactile sensation of surface roughness using ultrasonic vibration," in *Nippon Telegraph & Telephone Corporation*, 1995, pp. 1134–1139, ISBN: 1050-4729.

[20] L. Winfield, J. Glassmire, J. E. Colgate, and M. Peshkin, "T-PaD: Tactile pattern display through variable friction reduction," in *Northwestern University*, 2007, pp. 421–+, ISBN: 978-0-7695-2738-3.

[21] N. Huloux, C. Bernard, and M. Wiertlewski, "Estimating friction modulation from the ultrasonic mechanical impedance," *IEEE Transactions on Haptics*, vol. 14, no. 2, pp. 409–420, Apr. 2021, ISSN: 1939-1412. DOI: 10.1109/TOH.2020.3038937.

[22] E. Vezzoli *et al.*, "Friction reduction through ultrasonic vibration part 1: Modelling intermittent contact," *IEEE Transactions on Haptics*, vol. 10, no. 2, pp. 196–207, Apr. 2017, ISSN: 1939-1412. DOI: 10.1109/TOH.2017.2671432.

[23] F. Roël, "A better grasp on the asymmetrical adaptation of grip force in response to friction perturbations," M.S. thesis, Delft University of Technology, 2022. [Online]. Available: http://resolver.tudelft.nl/uuid:0f4bcfa4-32d7-41e8-91a5-0d30ae0f928d.

[24] R. S. Johansson and G. Westling, "Signals in tactile afferents from the fingers eliciting adaptive motor responses during precision grip," *Experimental Brain Research*, vol. 66, no. 1, pp. 141–154, Mar. 1, 1987, ISSN: 1432-1106. DOI: 10.1007/BF00236210. [Online]. Available: https://doi.org/10.1007/BF00236210.

APPENDIX A
DESIGN OF EXPERIMENTAL DEVICES

This appendix documents the design process of the experiment devices, including the torque-unloading structure, the constant force structure, the shoulder supporter, and the friction-reduction plates.

A. Design Criteria

The experiment system should be able to mimic a daily lifting task, where the subject grabs an object with a certain weight, lifts it to a certain height, with or without using upper-arm muscles, and holds it for a certain time. In the meantime, the system should be able to change the friction of the grasping object, record its position, and record the subject's pinching force. The system should be lightweight and minimalistic, with as few powered parts as possible.

The object should have at least 100 mm of effective movement range, with an adjustable weight between $\pm$ 5 N. The object should have a grasping area of approximately 30 $\times$ 30 mm. The system should be able to generate 10 - 20 N of force at the subject's wrist.

B. Torque-Unloading Structure

To measure the subjects' pinching force, the device employs 2 Futek LSB200 s-beam load cells due to their compact and lightweight design. However, being 1D force sensors, these load cells are prone to additional forces in other directions, which create torques and interfere with measured pinching force. Therefore, a torque-unloading structure should be designed to ensure the forces exerted on load cells are only in their working direction.

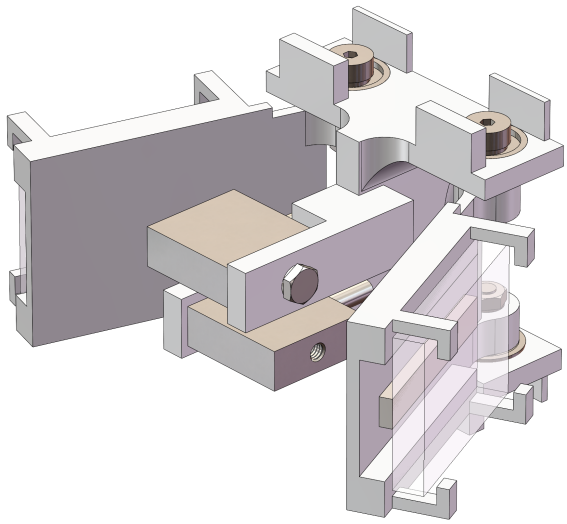

Fig. 17. The torque-unloading structure. 2 ball bearings were used to form a hinge between a pinching plate and the load cell frame. The glass plates can only transmit forces that are perpendicular to the direction of the sensor to the sensor.

The structure is shown in Fig. 17. The load cells are fixed in a support frame. Each plate that subjects will be pinching is connected to the frame via 2 ball bearings, forming a hinge structure. In this way, the movement of the pinching plates is confined to 1 degree of rotational freedom with respect to the support frame. And since the deformation of the load cells would be neglectable during loading conditions, the small rotational movement could be treated as a linear movement in the load cell's working direction. Therefore, only the pinching force would be recorded by the load cells.

Additionally, in this configuration, if the subject is pinching an off-center area of the plate, it might create additional torque due to the small flexibility of the 3D-printed frames. Therefore, the device uses 2 load cells to reduce the moment arm at the edge of the plates, thus minimizing this additional torque.

This structure along with the load cells and the friction modulation plates forms the pinching object. Fig. 17 shows its full assembly.

C. Constant Force Structure

To mimic daily tasks where people grab and lift objects with two fingers, a force should be applied to the pinching object and stay constant during the entire movement. Although the block has an intrinsic weight, this force should be easily adjustable, to create a controlled experimental setup, and to accommodate various experimental plans.

The simplest way is to attach an additional weight to the pinching object. This, however, would add weight to the whole device, compromising the lightweight design. Alternatively, a motor could apply a desired force on the object. But a powered component also adds a lot of complexity to the system, both in controlling and maintenance. Therefore, the device uses a spring-powered pulley system to exert the constant vertical force to achieve a simplistic design.

1) The Minimal System: The concept of the constant force structure is shown in Fig. 18. The pinching block is connected to a fixed frame via a parallel four-bar linkage system (ABCD), allowing it to move up and down without affecting its pose. A 0 free-length spring FG is attached to the midpoint F of the hinges B and D on the block. The other end of the spring is attached to the frame at G. Point E is the midpoint between A and C. This way, EF forms a virtual beam moving along with AB and CD in the parallel linkage system.

As the block moves, the elongated spring exerts a force F_{spring} on point F of the block. Given the spring has 0 free length, and the stiffness of the spring k, we have:

$$F_{spring} = kl_{FG} \tag{4}$$

F_{spring} can be decomposed into a component along the virtual beam EF and a vertical component, namely F_{beam} and F_y. Since EF is always parallel to AB and CD, F_{beam} will be passed to the frame, leaving only F_y on the block. Consider the vector triangle of F_{spring}, F_{beam}, and F_y, since they are always parallel to FG, EF, and EG, respectively, regardless of the block's position, we have:

$$\triangle EFG \sim \triangle F_{spring}F_{beam}F_y \tag{5}$$

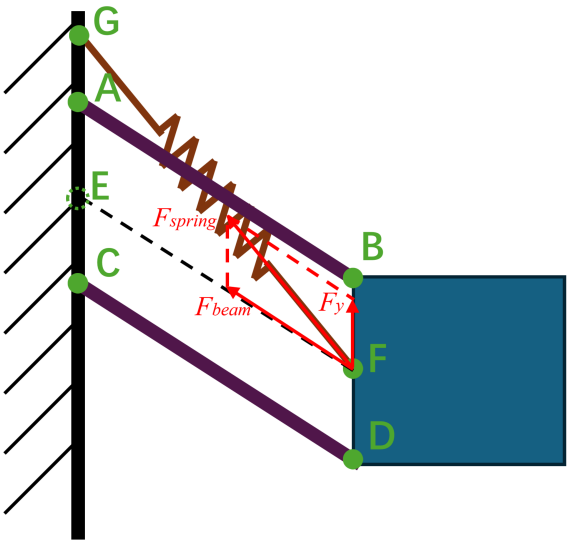

Fig. 18. The concept of the constant force structure. The black lines, purple lines, green dots, brown zig-zag lines, and the blue box represent the fixed frame, linkage bars, hinges, the spring, and the pinching block, respectively. The red vectors are the diagram of the spring's pull on the block.

This gives us:

$$\frac{F_y}{l_{EG}} = \frac{F_{spring}}{l_{GF}} \tag{6}$$

Substituting (6) with (4), we now have:

$$F_y = kl_{EG} \tag{7}$$

This system has these interesting properties:

1) Once the position of the spring attachment point G on the frame is set, the block will be acted on by a constant vertical force throughout its range of motion.
2) The said vertical force can be easily adjusted by tuning the distance between E and G.

2) Zero Free-length Spring: The above concept requires a 0 free-length spring to work (consider (4), it would not work with an additional term). However, real-world springs have these complications:

1) A realistic spring inevitably has a physical length l_0, then F_{spring} would become $k(l_{GF} - l_0)$ (Fig. 19a purple line).
   The solution is to move the spring out of the space FG. This way the spring outputs force as soon as l_{GF} increases (Fig. 19a blue line).
2) Most tension springs are manufactured with a built-in tension F_0. That is, the spring only starts to elongate when the applied tension is above a threshold. This way, F_{spring} would become $kl_{GF} + F_0$ (Fig. 19b purple line). This is solved by applying a pre-tension $F_{pre} = F_0$. This would ensure the spring elongates once an additional force has been applied (Fig. 19b blue line).

The device implements the above solutions with a pulley system (Fig. 20). E, F, G, H, and I are pulley wheels. The pulley system uses pulleys of the same size to eliminate the impact of pulley size on the system. E, F, and G are equivalent

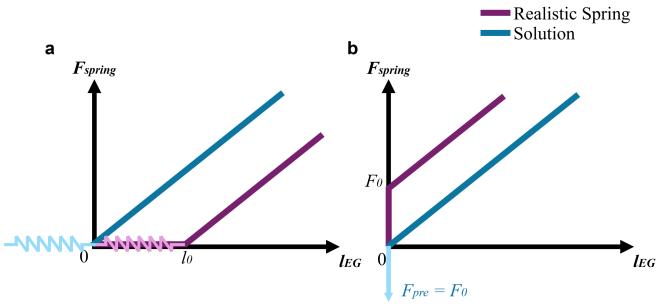

Fig. 19. Force-length relationship of realistic springs (purple lines) and corresponding solutions. a) a spring with a physical length. b) a spring with a built-in tension.

to the corresponding points in the minimal system depicted in Fig. 18. One end of the cable is fixed at G, while the other end is connected to the spring. The other end of the spring is connected to a bolt J, which is screwed into the fixed frame.

In this configuration, the length of the cable and spring combined in the interval FEHIJ is constant regardless of the block's position. When the block moves, only the length of the cable between F and G changes. This allows the spring to be effectively seen as if placed between F and G, while completely not taking any physical space in that interval. Since cable EF is parallel to the beams, its tension is completely supported by them. Now, this pulley system can be seen as equivalent to the aforementioned minimal system, thus providing the desired constant vertical force as discussed before. Furthermore, the pre-tension of the spring can be easily and accurately adjusted by driving the bolt in or out of the frame, solving problem 2.

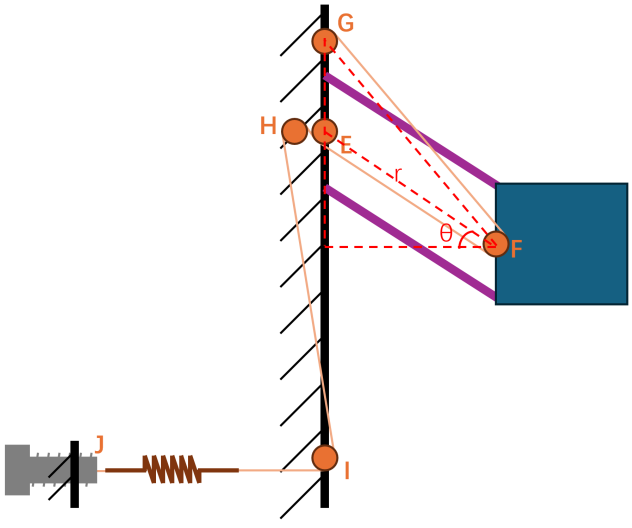

Fig. 20. The pulley system used to tackle realistic spring problems. Brown circles represent pulley wheels while brown lines represent pulley cables. The spring is connected to the cable at one end, and to a bolt at the other end.

3) Adjustable Vertical Force: According to 7, the vertical force can be adjusted by changing the distance between E and G. This is achieved by implementing a simple lead screw mechanism. Observe Fig. 20, to enable wheel G to move

across wheel E, they must not exist on the same plane. Thus instead of a wheel, F was made a cylinder that intersects both planes, to allow smoother cable transition (Fig. 21).

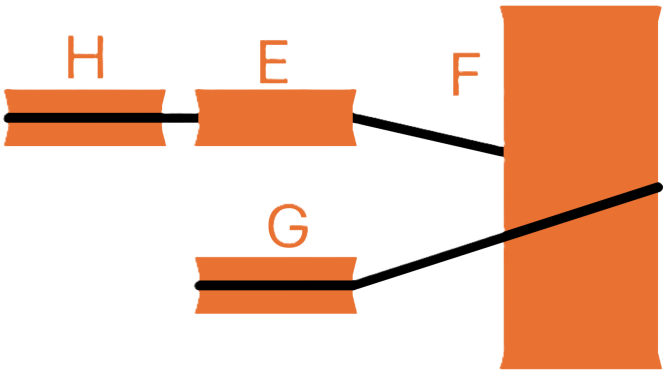

Fig. 21. The top view of pulley wheels E, F, G, and H. G and E, H are not in the same plane. F was made a cylinder to allow smoother cable translation.

4) Spring Specification: The stiffness of the spring was selected by these design criteria:

1) The net vertical force should be adjustable between ± 5 N. A preliminary evaluation using SolidWorks showed that the pinching block weighs approximately 150 g. So the total maximum vertical force should be at least 6.5 N.
2) The linkage system should be able to move up to ± 75 degrees (respective to the horizontal plane) in order to build a 100 mm movement range without a too large curvature.
3) The movement of the slider wheel G (as in Fig. 20) should not exceed l_{EG} = 20 mm from its neutral position. This is to ensure the design is compact.

The linkage beam length r was set to be 50 mm, to mimic a simple daily pinch-lift task. Given the angle between a linkage beam and the horizontal θ (in degrees), it is clear that:

$$(l_{EG} + r\sin\theta)^2 + (r\cos\theta)^2 = l_{FG}^2 \tag{8}$$

Substituting (8) with (6), we have:

$$F_{spring} = \frac{\sqrt{(l_{EG} + r\sin\theta)^2 + (r\cos\theta)^2}}{l_{EG}} F_y \tag{9}$$

With the boundary conditions:

$$\begin{cases} F_y > 6.5 \text{ N} \\ \theta > 75 \text{ degrees} \\ l_{EG} < 20 \text{ mm} \end{cases} \tag{10}$$

We have $F_{springMax} > 22.59$ N. $F_{springMax}$ = 23 N was chosen to leave some redundancy to the system. Therefore we have $k > 1.15$ N/mm. The final design uses a Tevema T31115D spring.

5) Spring Characterization and Calibration: To character the spring, its length was measured with a Mitutoyo caliper (d = 0.05 mm) after freely suspending different weights on it. The mass of the weights was measured by a KERN PFB 3000-2 scale (d = 0.01 g). Fig. 22 shows the force-length relationship of this spring.

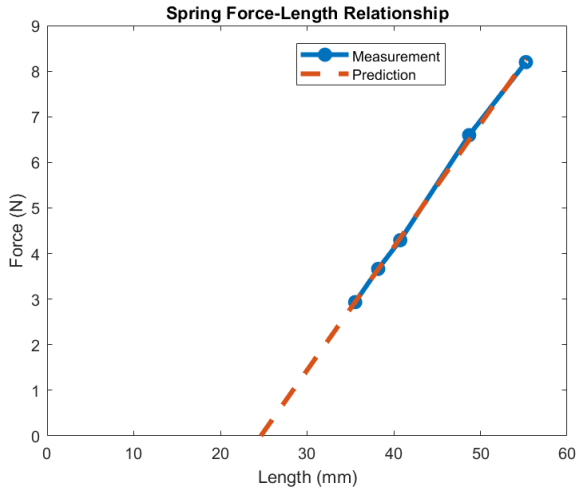

Fig. 22. The force-length relationship of the spring used in this experiment. The blue line is the measured data, while the orange dashed line is the predicted profile using linear regression.

A linear regression gives the predicted relationship (units: N, mm):

$$\hat{F}_{T31115D} = 0.2699 \times l_{T31115D} - 6.6572 \tag{11}$$

Its intercept on the x-axis is 24.6625 mm. This means the spring's free length (when the output force is 0) would be 24.6625 mm.

To calibrate the spring, first adjust the height of pulley wheel G in Fig. 20 to coincide with wheel G. This way, the length of the imaginary spring at GF is known to be 50mm. Now, assuming the imaginary spring has 0 free length, the actual spring's length should be its free length plus 50mm, which is 74.6625 mm. Thus, the spring was pre-elongated to 75 mm (rounded) to complete its calibration.

D. Elbow Perturbation Structure

The elbow support was designed to be a simple non-powered device, to maximize its safety and reliability. The design uses aluminum profiles as the frame, due to their high versatility and stability. To provide enough torque to perturb the subject's elbow, the design uses torsion springs. They have a linear angle-torque response and can go under enormous duty cycles without fatigue.

The final design is shown in Fig. 6. 4 profiles form a rectangular base to ensure the stability of the device. A profile is fixed vertically to raise the arm support (the long profile attached to it) above the table height. Fig. 6a is a hinge that connects the vertical profile to the arm support. The hinge only allows the arm support to rotate counter-clockwise (from the top view) and blocks its movement in the other direction. The yellow rod in Fig. 6b is connected to the vertical profile. Two torsion springs (TV01740R, made by Tevema, 5.75 N·mm/degree) were slid onto the rod, with one foot blocked by the vertical profile, and the other fixed on the

arm support. This way they can provide a clockwise torque to the arm support. They are pre-tensioned by approximately 330 degrees, so they will provide 4.14 N·m of torque when the subject's elbow is flexed to 30 degrees. This results in a force of 1.242 N on the wrist, assuming a lower arm length of 0.3 m. Fig. 6c is a 3D-printed wrist holder fixed on the arm support. Its position can be adjusted to fit the subject's arm length. There are no rigid confinement mechanisms on the holder, to maximize the subject's movement flexibility and safety.

During an experiment, the subject places their elbow on Fig. 6a and their wrist on Fig. 6c. The constant-force device will be fixed on the arm support in front of Fig. 6c.

E. friction modulation Plates

1) Glass Plates: The friction modulation surfaces need to vibrate at a very high frequency ($>$ 30 kHz) to provide proper friction reduction. So its materials should have good resonance properties, with a high Young's modulus to avoid damping. This design uses borosilicate glass plates manufactured by Glasatelier Saillart for such purpose. This material has the following mechanical properties: Young's modulus E = 6.2 $\times$ 10^{10} Pa, density ρ = 2400 kg/m^3.

As the subject should hold firmly onto the object, their fingers would not be moving relative to the glass plates. So the friction-reduction plates could be as small as the area of a human fingerpad. The initial design chose an approximate dimension of 30 $\times$ 30 mm for these plates. Due to this relatively small size, 1 single resonance nodal line would be sufficient to reduce friction. According to [25], the thicker the glass plates, the lower the decay in the mass-spring-damper system will be, thus the thickness of the glass plates was chosen as h = 5 mm. To make the resonance nodal line as straight as possible, the length of one side of the glass plate l_r should be an integral multiple (n) of the vibration wavelength λ to maximize resonance, while the length of its adjacent side l_{ar} should be $(n + 0.5)\lambda$ to minimize resonance on this direction [25].

The glass plates are attached to the pinching object by elastic press fit into rectangular clamps padded with rubber, as Fig. 17 shows (rubber padding not rendered).

2) Analytical Model: [25] described an analytical model based on Bernoulli's theory of transverse vibrations, to calculate the relationship between the resonance frequency ω and resonate side length l_r:

$$\cos(\beta l_r)\cosh(\beta l_r) - 1 = 0 \tag{12}$$

While

$$\beta = \sqrt[4]{\frac{12\rho\omega^2}{Eh^2}} \tag{13}$$

A frequency ω = 40 kHz was assumed. Solving (12) with the material and dimension properties discussed above gives the minimum l_r = 34 mm (node number being 1) while λ = 17 mm. This gives the anti-resonance side length l_{ar} = 25.5 mm. The piezoelectric actuator should be placed on a nodal line, and since only 1 is present, it should be placed in the middle of the glass plates.

3) Piezoelectric Actuators: The vibration of the glass plates needs to be provided by piezoelectric actuators. Specifically, since this device would benefit from straight nodal lines, rectangular-shaped piezoelectric actuators would fit it the best. These actuators are as simple as a chunk of piezoelectric ceramic covered with conductive layers on two opposing sides as electrodes. Once they are applied with alternating voltage, the ceramic would stretch and shrink at the same frequency, and provide the high-frequency vibration. Dimensions of the actuators were chosen from the manufacturer Steminc's catalog. The final design uses model SMPL60W05T21F27R. Its dimensions are 60 $\times$ 5 $\times$ 2.1 mm. They were cut to 34 mm lengthwise to fit the glass plates. It is made of Steminc's material SM111. It is glued on the glass plates with 3M Scotch-Weld epoxy adhesive DP490.

4) Finite Element Model: A finite element model (FEM) built with COMSOL further validates the calculated results. The geometry of the model is in Fig. 23a. The FEM studied its frequency response from 20 to 60 kHz. The result showed 2 peaks in displacement (*i.e.* vibration amplitude): a higher one around 35.8 kHz, and a lower one around 21.6 kHz (Fig. 23b). The higher the vibration amplitude, the thicker the squeeze film, thus the better the friction-reduction effect. Fig. 23c and Fig. 23d show their mode shapes respectively. The results suggest that the mode shape under 35.8 kHz has the desired direction (nodal line alongside the resonance side), while the one under 21.6 kHz has the opposite direction.

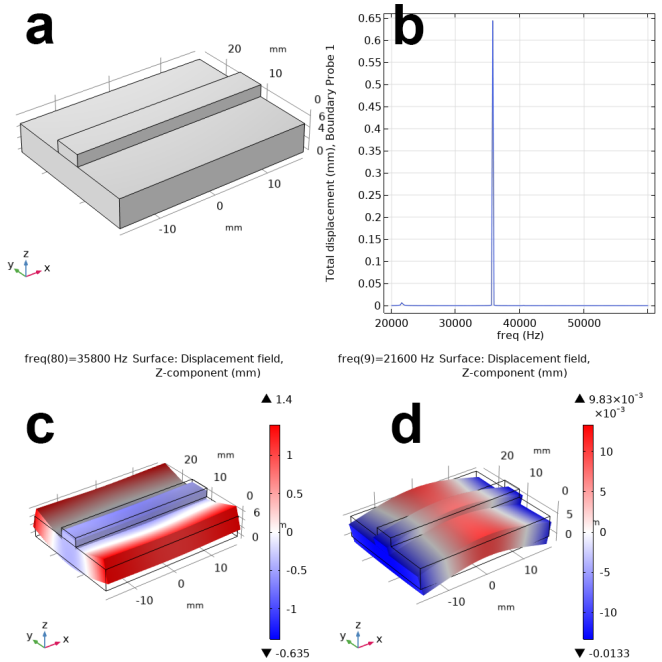

Fig. 23. FEM analysis of the friction-reduction plate. a) The geometry of the FEM model. The large plate underneath is the glass plate, while the small plate on top is the piezoelectric actuator. b) The glass plate's displacement under different excitation frequencies. c) The mode shape under 35.8 kHz. d) The mode shape under 21.6 kHz.

5) Vibrometer Testing: The physical assemblies of the 2 friction modulation plates were characterized using a Polytec OFV-5000 laser vibrometer. The test set used a Tektronix

AFG1062 function generator to generate excitation signals, a PiezoDrive PD200 amplifier to amplify the signal, and a Keysight InfiniiVision DSOX2014A digital oscilloscope to display the readings from the vibrometer. The frequency response around 35.8 and 21.6 kHz were qualitatively tested. Surprisingly, the previously determined desired frequency (35.8 kHz) yields very slight friction-reduction effects, while the unexpected mode shape under 21.6 kHz showed ample friction-reduction effects. The reason behind this might be that the dimensions of this experiment's friction modulation plates are too small compared to previous studies (165.3 $\times$ 149.8 mm in [25], 68 $\times$ 52 mm in [23]), so the size effect dominates over the theoretical model. Anyhow, this phenomenon was not further studied since it's not in the scope of this thesis. No significant drawbacks were observed from the 21.6 kHz vibration mode over the 35.8 kHz one. Therefore, further tests and experiments use excitation signals around 21.6 kHz, due to this frequency's better practical performance.

This test further quantitatively characterized the 2 friction modulation plates. The excitation signal used an amplitude of 10 V. The signal was amplified 20 times before being applied to the actuators. The plates were placed on a sponge to provide damping. The vibrometer detects the plate's vibration velocity and outputs an analog voltage signal of 50 mm/s/v. The frequency response was scanned around 21.6 kHz to determine the optimal frequency with the highest vibration amplitude. The data were measured at the center of the plates. Table II shows the testing results (vibrometer output already converted to physical quantities).

TABLE II
CHARACTERIZATION OF FRICTION MODULATION PLATES

	Plate A	Plate B
Optimal Frequency (kHz)	23.4	23.1
Vibration Velocity Amplitude (mm/s)	912.5	831.25
Vibration Displacement Amplitude (μm)	6.21	5.72

The key performance indicator, vibration displacement amplitude, is the integral of vibration velocity of a half period. The calculation results are also in Table II. A more accurate indicator could be the change of friction coefficient, but this has proven to be influenced by many factors [21, 22], and is complicated to measure or derive, so it is not included in the scope of this thesis. From an empirical point of view, $\tilde{6}$ μm of vibration can already result in a very satisfactory friction reduction effect [21, 22].

During the experiments, the same function generators and amplifiers (a Tektronix AFG1062 and two PiezoDrive PD200) are used. However, due to resource problems, they were switched to two RSPRO RSDG 830 and two Falco Systems WMA-300 respectively. The output voltages are tuned to be the same to keep a consistent vibration amplitude.

REFERENCES

[21] N. Huloux, C. Bernard, and M. Wiertlewski, "Estimating friction modulation from the ultrasonic mechanical impedance," *IEEE Transactions on Haptics*, vol. 14, no. 2, pp. 409–420, Apr. 2021, ISSN: 1939-1412. DOI: 10.1109/TOH.2020.3038937.

[22] E. Vezzoli *et al.*, "Friction reduction through ultrasonic vibration part 1: Modelling intermittent contact," *IEEE Transactions on Haptics*, vol. 10, no. 2, pp. 196–207, Apr. 2017, ISSN: 1939-1412. DOI: 10.1109/TOH.2017.2671432.

[23] F. Roël, "A better grasp on the asymmetrical adaptation of grip force in response to friction perturbations," M.S. thesis, Delft University of Technology, 2022. [Online]. Available: http://resolver.tudelft.nl/uuid:0f4bcfa4-32d7-41e8-91a5-0d30ae0f928d.

[25] T. Brans, "Pseudo Potential Fields on Surface-Haptic Touchscreens using Friction Modulation," M.S. thesis, Delft University of Technology, 2022. [Online]. Available: http://resolver.tudelft.nl/uuid:5f680e80-5411-4784-b3c5-831f7db59d8b.

APPENDIX B
RAW DATA OVERVIEW

Fig. 24 stacks all the trial data (before exclusion) to show their distribution. Each line indicates the grasping force over time of a single trial. It is clear that most trials' grasping force range falls between 0 - 5 N. Fig. 25 further shows the distribution of the maximum force of each trial.

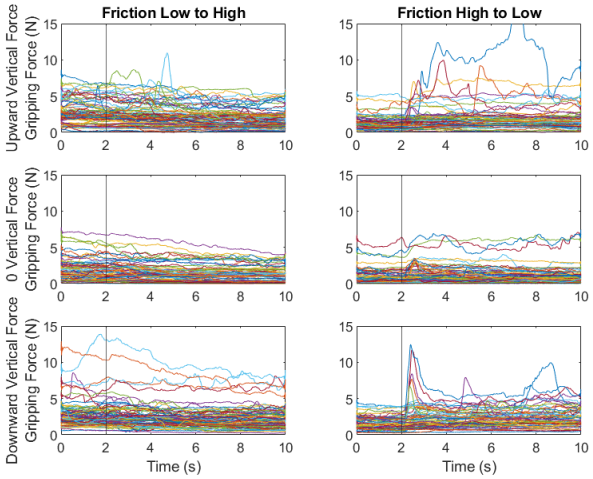

Fig. 24. Overview of all the trial data. Each line indicates a single trial. The left column indicates when the friction changes from low to high, while the right one indicates otherwise. The rows from top to bottom indicate 0.5 N upward, 0 N, and 0.5 N downward force on the object respectively.

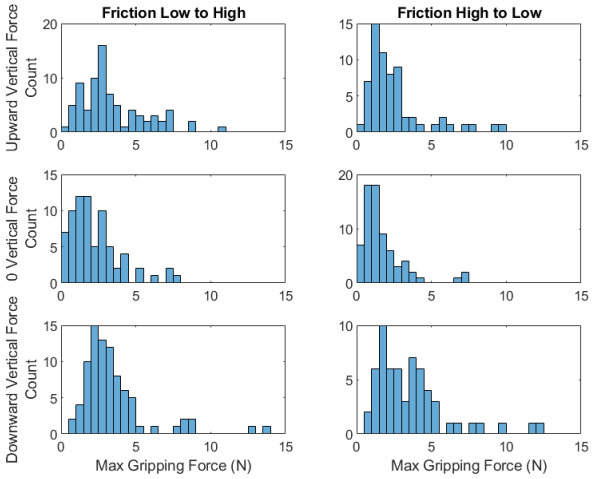

Fig. 25. Distribution of the max force of each trial. The left column indicates when the friction changes from low to high, while the right one indicates otherwise. The rows from top to bottom indicate 0.5 N upward, 0 N, and 0.5 N downward force on the object respectively.

Several human errors may occur during a trial. Fig. 26 shows all the grasping force data where the friction changes from high to low, and the object has a downward vertical force (the lower right figure in Fig. 24). It represented two types of human errors. a) Shows that the subject overreacted when they first felt the friction change. b) Shows that the subject lost concentration on grasping at some point during a trial, and suddenly tried to secure the object. As they both reached an unrealistic value during the trial, a threshold was used to detect these errors. The value was determined by 10 times the minimum grasping force needed at the low friction condition (8.56 N, represented by the dashed vertical line in Fig. 26). Further analysis excludes all trials with force exceeding this threshold. 12 trials were excluded in total among 432 trials.

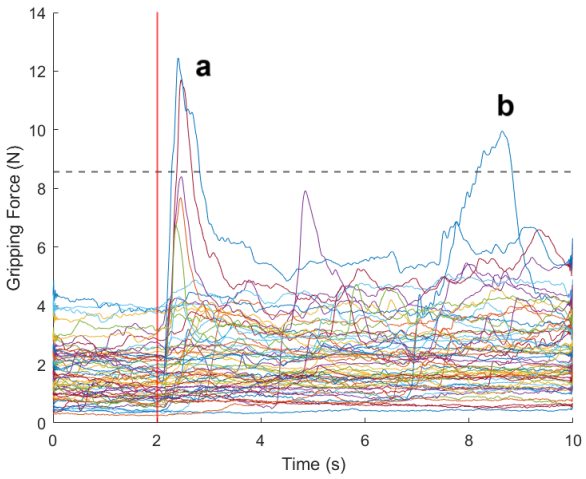

Fig. 26. All the grasping force data where the friction changes from high to low, and the object has a downward vertical force. The vertical red lines indicate the time of the friction change (2 s). The horizontal dashed line shows the threshold of data exclusion (8.56 N). a) The subject overreacts to the friction change. b) The subjects lost concentration during a trial.

APPENDIX C
DOCUMENTARY QUIZ

Nature Lives and Nature Environments Final Exam

0 ECTS

1. What is Antarctica like?
    a. Ice caps floating and colliding on the raging sea
    b. Vast expanse of whiteness with sparkles of vibrant colors
    c. Freezing cold yet life thrives
    d. All of the above

2. What creatures dwell in this frozen world?
    a. Lovely penguins
    b. Magnificent humpbacks
    c. Ruthless orcas
    d. Wandering albatrosses
    e. All of the above

3. What are the sufferings of their lives?
    a. Harsh extreme conditions
    b. Cruel prey-predator relationship
    c. Devastating climate change
    d. All of the above

4. Should we do what we can to preserve this frozen world?
    a. Yes
    b. No

5. Would you like to visit there one day? (Optional: briefly explain)
    a. Yes
    b. No

APPENDIX D
MECHANICAL DRAWINGS

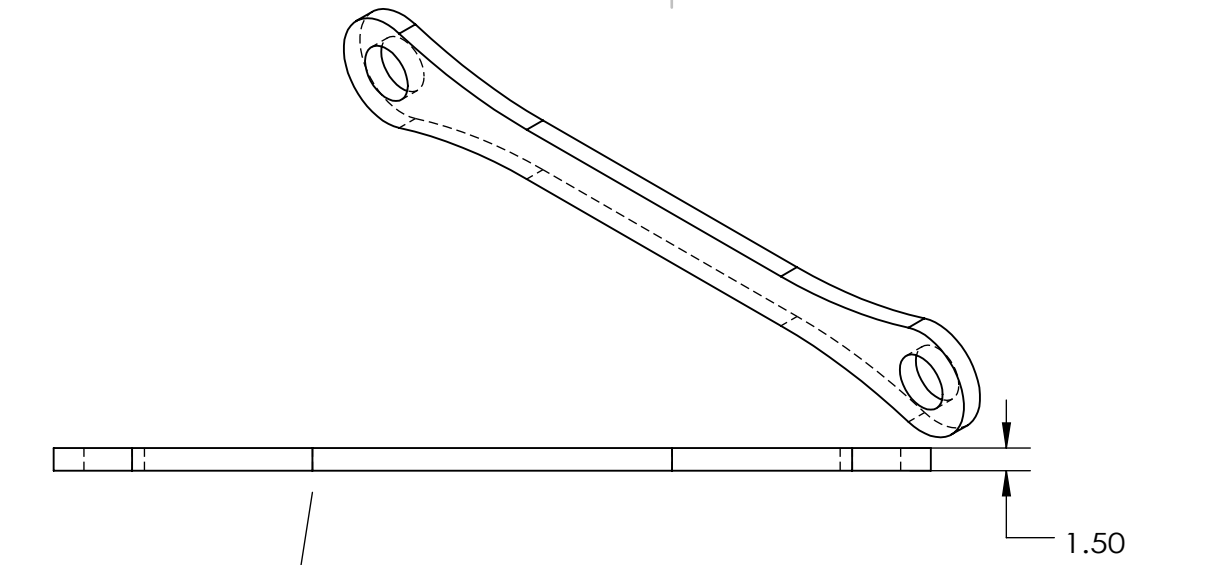

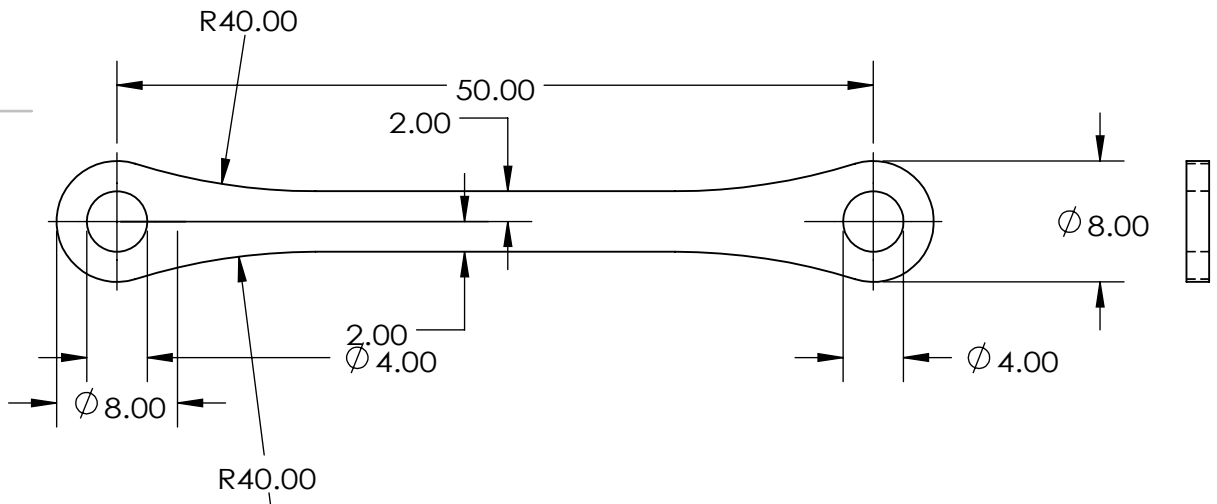

UNLESS OTHERWISE SPECIFIED: DIMENSIONS ARE IN MILLIMETERS SURFACE FINISH: TOLERANCES: LINEAR: ANGULAR:	FINISH: LASER CUT	DEBURR AND BREAK SHARP EDGES	DO NOT SCALE DRAWING / REVISION

	NAME	SIGNATURE	DATE
DRAWN			
CHK'D			
APPV'D			
MFG			
Q.A			

TITLE:

MATERIAL: 3.3535 (EN-AW 5754)

DWG NO. Arm

A4

WEIGHT: 1.05

SCALE:2:1

SHEET 1 OF 1

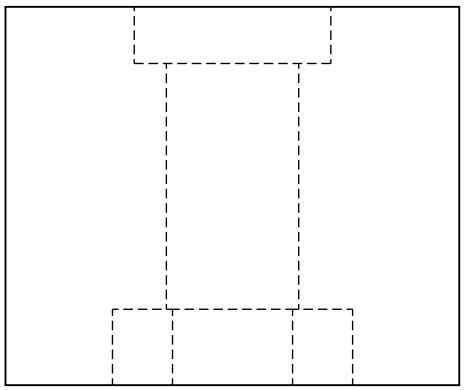

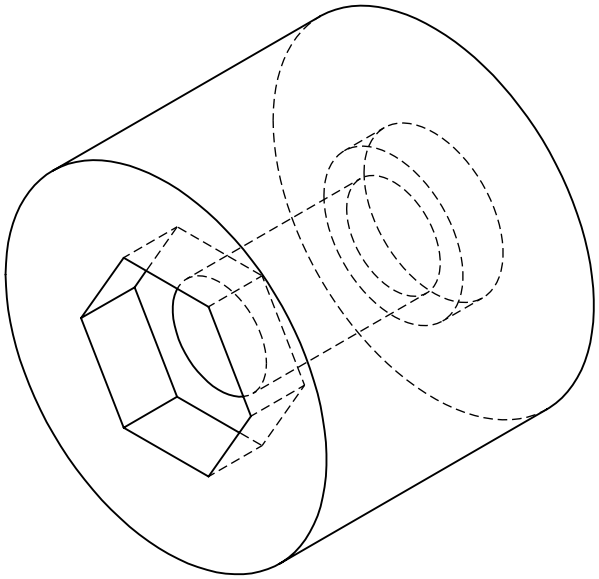

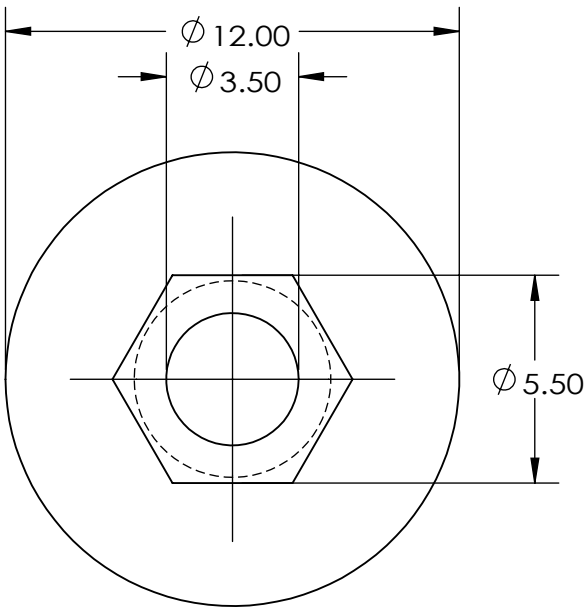

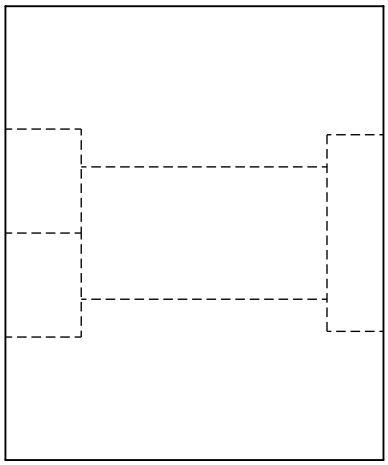

UNLESS OTHERWISE SPECIFIED: DIMENSIONS ARE IN MILLIMETERS SURFACE FINISH: TOLERANCES: LINEAR: ANGULAR:	FINISH: FDM 3D PRINTED	DEBURR AND BREAK SHARP EDGES	DO NOT SCALE DRAWING / REVISION

	NAME	SIGNATURE	DATE
DRAWN			
CHK'D			
APPV'D			
MFG			
Q.A			

TITLE:

MATERIAL: PLA

DWG NO. Magnet Holder

A4

WEIGHT:

SCALE:5:1

SHEET 1 OF 1

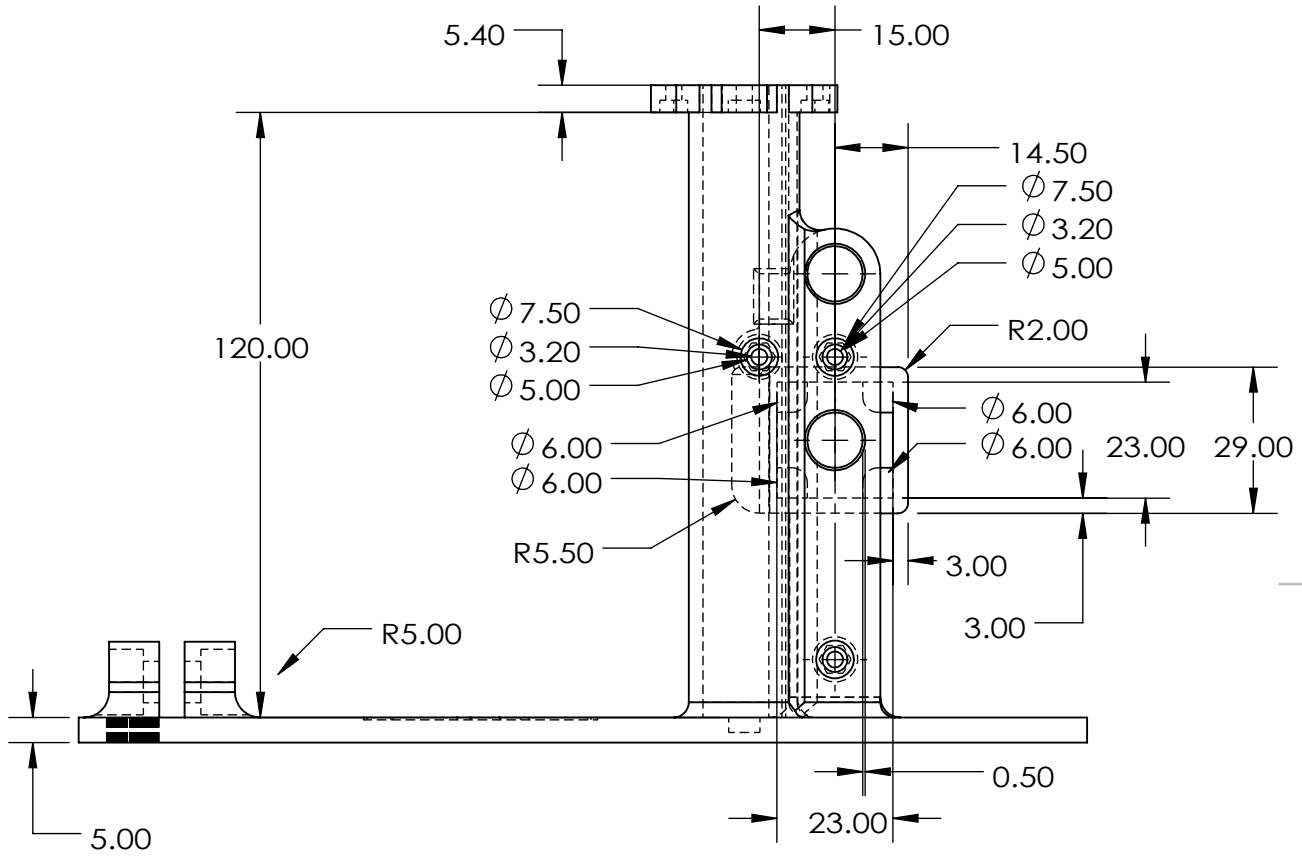

UNLESS OTHERWISE SPECIFIED: DIMENSIONS ARE IN MILLIMETERS SURFACE FINISH: TOLERANCES: LINEAR: ANGULAR:	FINISH: FDM 3D PRINTED	DEBURR AND BREAK SHARP EDGES	DO NOT SCALE DRAWING / REVISION

	NAME	SIGNATURE	DATE
DRAWN			
CHK'D			
APPV'D			
MFG			
Q.A			

TITLE:

MATERIAL: PLA

DWG NO. Main Frame

A4

WEIGHT: 122.41

SCALE:1:1.5

SHEET 1 OF 3

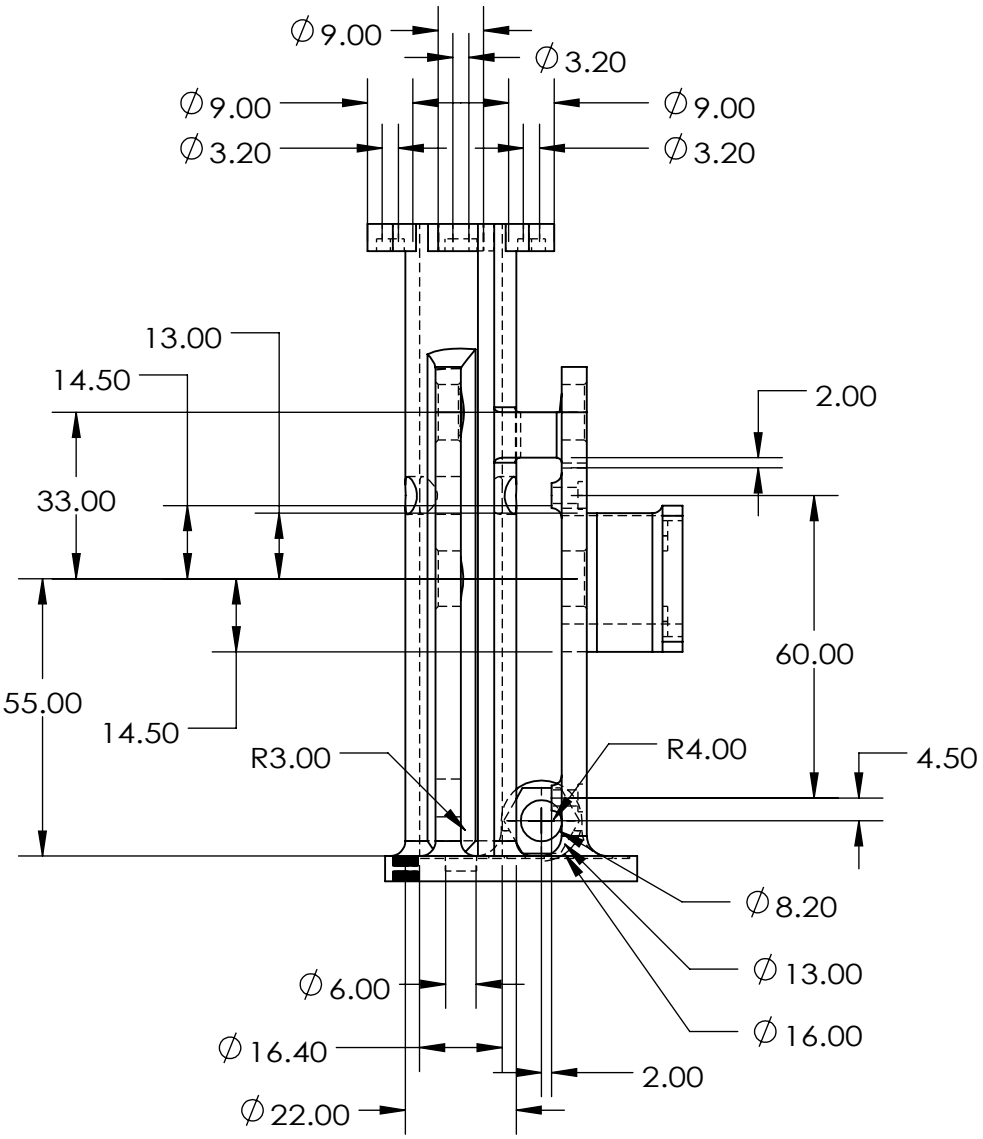

UNLESS OTHERWISE SPECIFIED: DIMENSIONS ARE IN MILLIMETERS SURFACE FINISH: TOLERANCES: LINEAR: ANGULAR:	FINISH: FDM 3D PRINTED	DEBURR AND BREAK SHARP EDGES	DO NOT SCALE DRAWING / REVISION

	NAME	SIGNATURE	DATE
DRAWN			
CHK'D			
APPV'D			
MFG			
Q.A			

TITLE:

MATERIAL: PLA

DWG NO. Main Frame

A4

WEIGHT: 122.41

SCALE:1:1.5

SHEET 2 OF 3

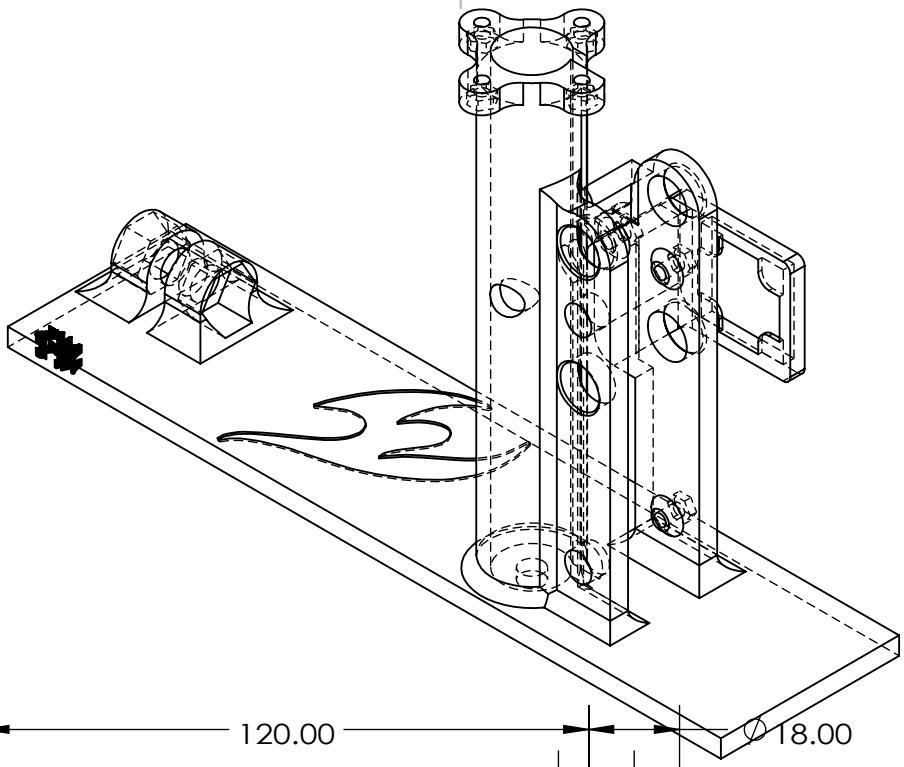

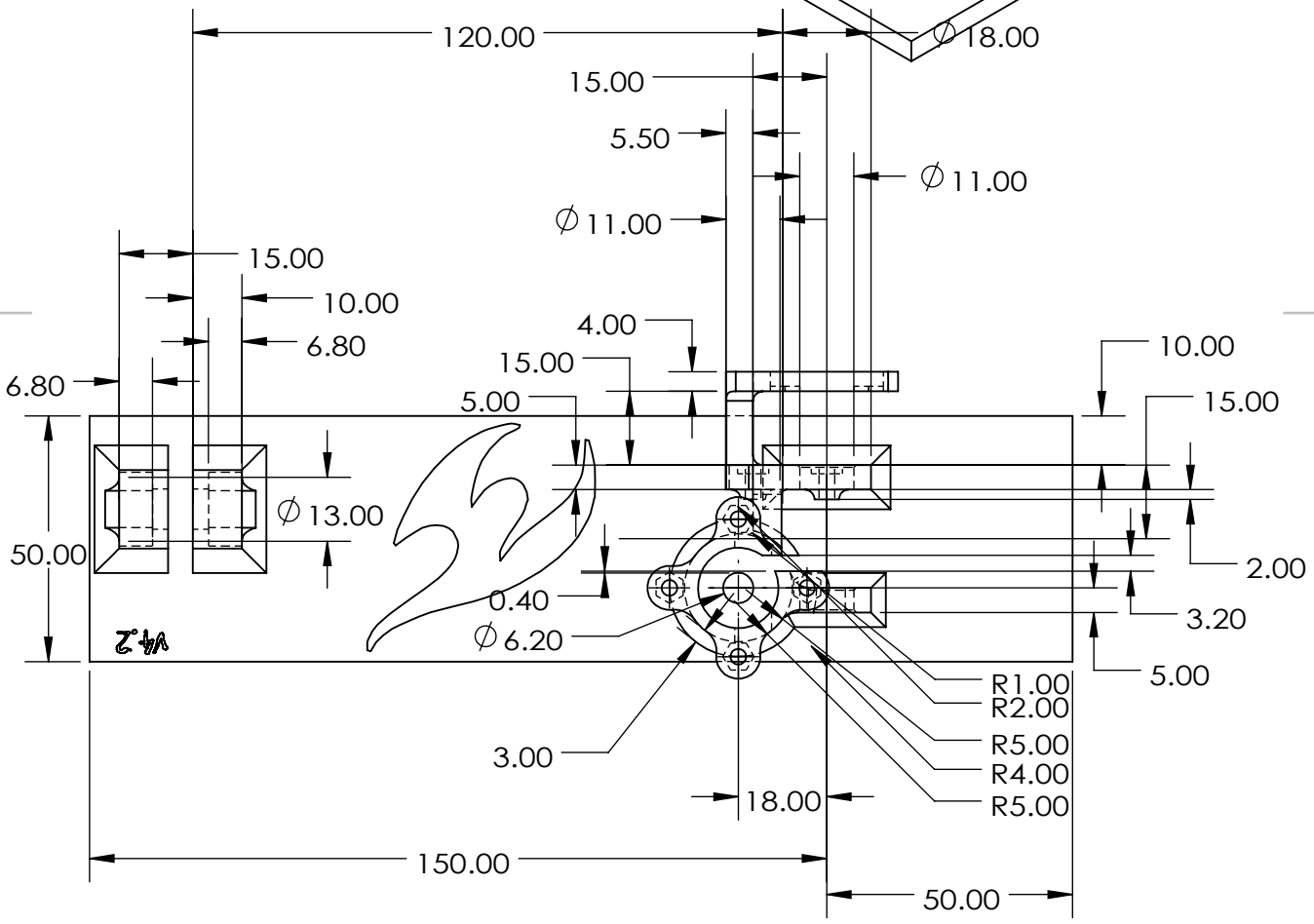

UNLESS OTHERWISE SPECIFIED: DIMENSIONS ARE IN MILLIMETERS SURFACE FINISH: TOLERANCES: LINEAR: ANGULAR:	FINISH: FDM 3D PRINTED	DEBURR AND BREAK SHARP EDGES	DO NOT SCALE DRAWING / REVISION

	NAME	SIGNATURE	DATE
DRAWN			
CHK'D			
APPV'D			
MFG			
Q.A			

TITLE:

MATERIAL: PLA

DWG NO. Main Frame

A4

WEIGHT: 122.41

SCALE:1:1.5

SHEET 3 OF 3

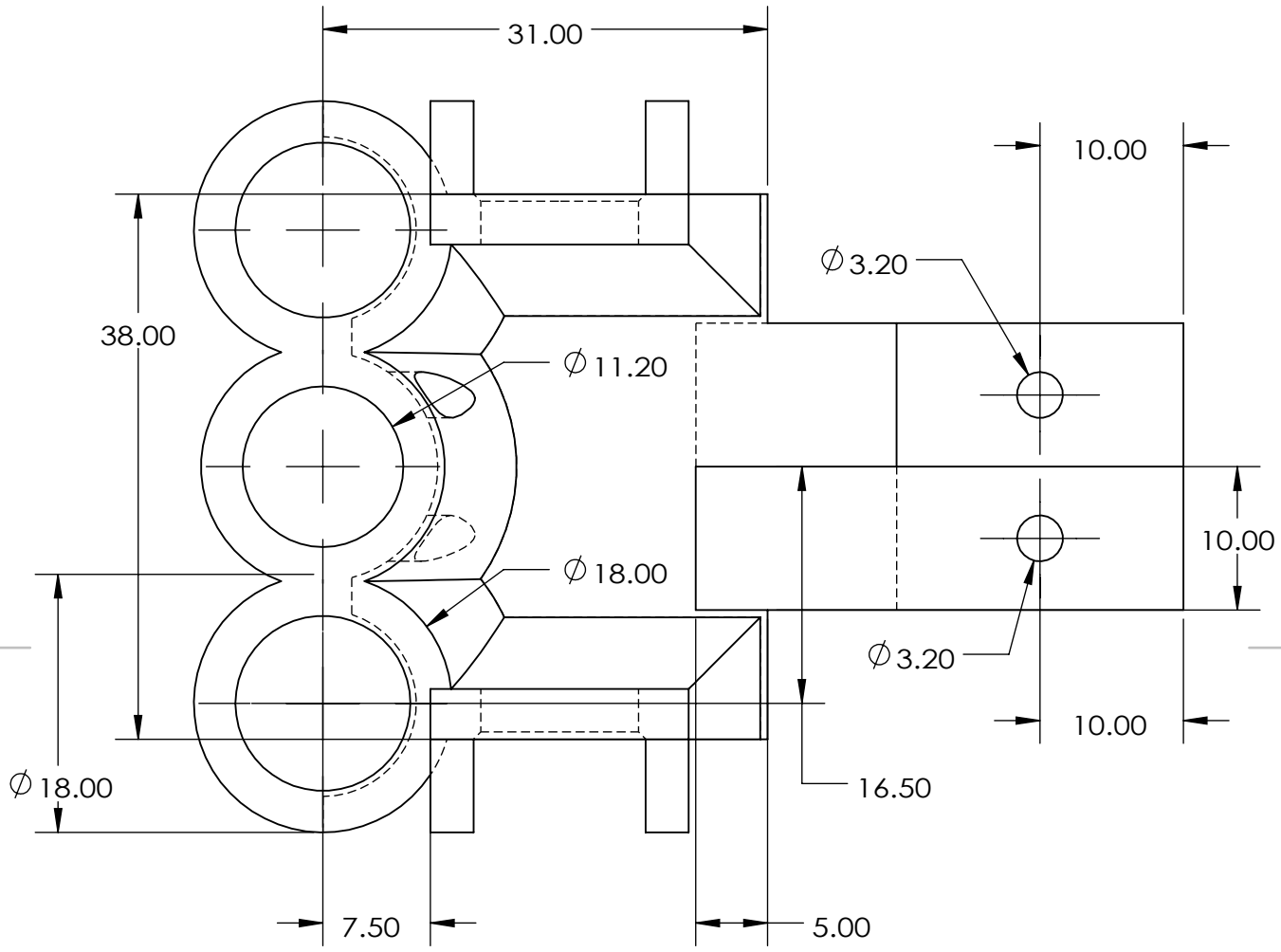

UNLESS OTHERWISE SPECIFIED: DIMENSIONS ARE IN MILLIMETERS SURFACE FINISH: TOLERANCES: LINEAR: ANGULAR:	FINISH: FDM 3D PRINTED	DEBURR AND BREAK SHARP EDGES	DO NOT SCALE DRAWING / REVISION

	NAME	SIGNATURE	DATE
DRAWN			
CHK'D			
APPV'D			
MFG			
Q.A			

TITLE:

MATERIAL: PLA

DWG NO. Object Frame

A4

WEIGHT: 27.40

SCALE:2:1

SHEET 1 OF 4

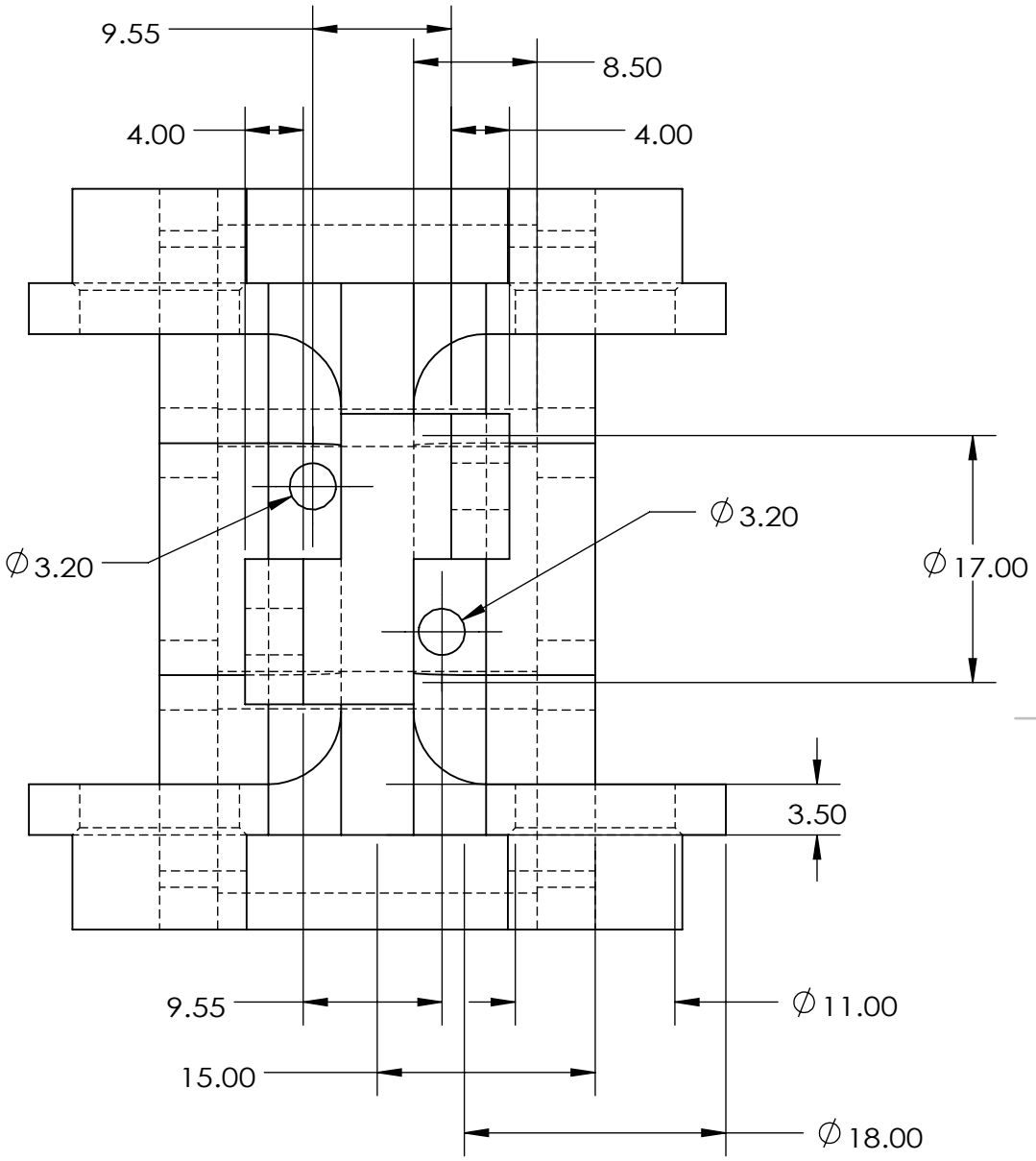

UNLESS OTHERWISE SPECIFIED: DIMENSIONS ARE IN MILLIMETERS SURFACE FINISH: TOLERANCES: LINEAR: ANGULAR:	FINISH: FDM 3D PRINTED	DEBURR AND BREAK SHARP EDGES	DO NOT SCALE DRAWING / REVISION

	NAME	SIGNATURE	DATE
DRAWN			
CHK'D			
APPV'D			
MFG			
Q.A			

TITLE:

MATERIAL: PLA

DWG NO. Object Frame

A4

WEIGHT: 27.40

SCALE:2:1

SHEET 2 OF 4

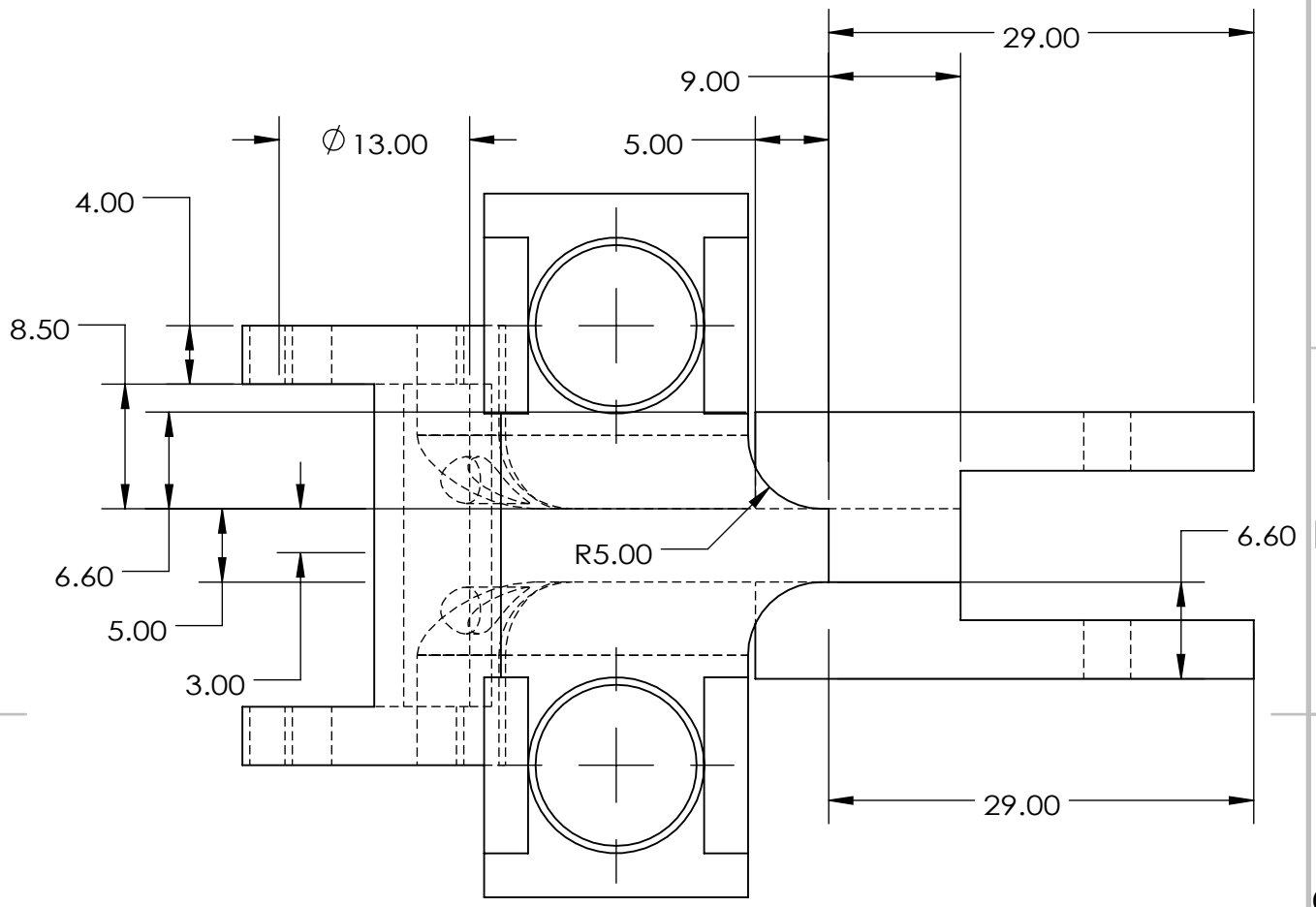

UNLESS OTHERWISE SPECIFIED: DIMENSIONS ARE IN MILLIMETERS SURFACE FINISH: TOLERANCES: LINEAR: ANGULAR:	FINISH: FDM 3D PRINTED	DEBURR AND BREAK SHARP EDGES	DO NOT SCALE DRAWING / REVISION

	NAME	SIGNATURE	DATE
DRAWN			
CHK'D			
APPV'D			
MFG			
Q.A			

TITLE:

MATERIAL: PLA

DWG NO. Object Frame

A4

WEIGHT: 27.40

SCALE:2:1

SHEET 3 OF 4

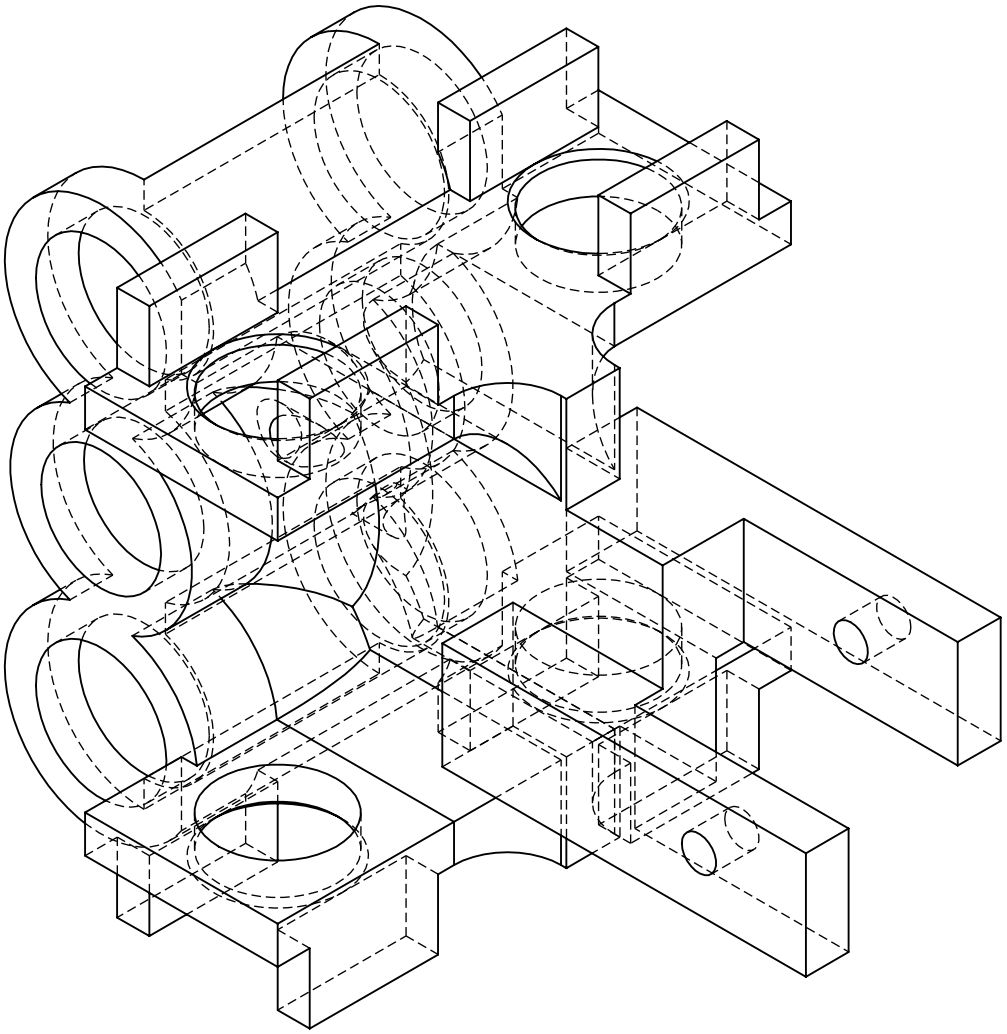

UNLESS OTHERWISE SPECIFIED: DIMENSIONS ARE IN MILLIMETERS SURFACE FINISH: TOLERANCES: LINEAR: ANGULAR:	FINISH: FDM 3D PRINTED	DEBURR AND BREAK SHARP EDGES	DO NOT SCALE DRAWING / REVISION

	NAME	SIGNATURE	DATE
DRAWN			
CHK'D			
APPV'D			
MFG			
Q.A			

TITLE:

MATERIAL: PLA

DWG NO. Object Frame

A4

WEIGHT: 27.40

SCALE:2:1

SHEET 4 OF 4

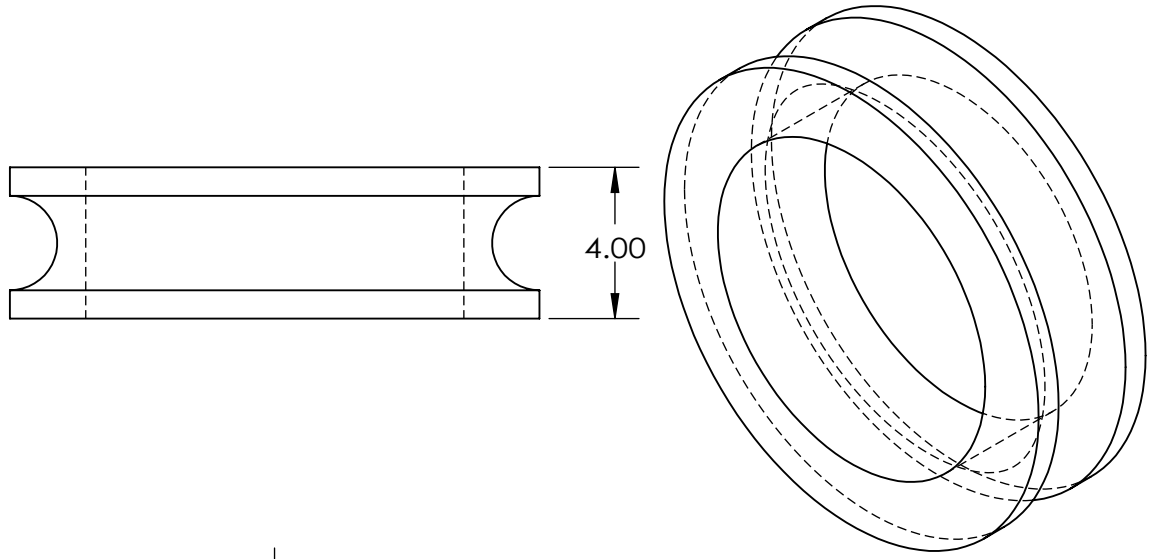

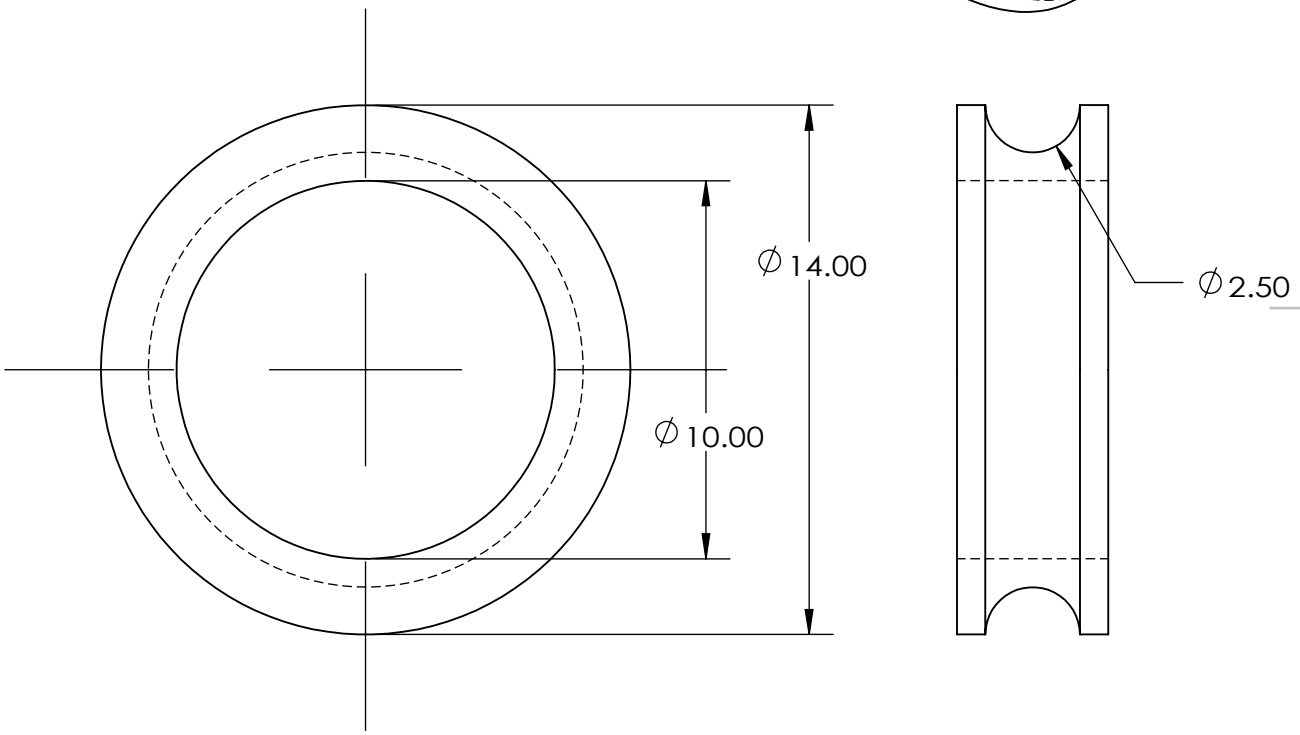

UNLESS OTHERWISE SPECIFIED: DIMENSIONS ARE IN MILLIMETERS SURFACE FINISH: TOLERANCES: LINEAR: ANGULAR:	FINISH: SLA 3D PRINTED	DEBURR AND BREAK SHARP EDGES	DO NOT SCALE DRAWING / REVISION

	NAME	SIGNATURE	DATE
DRAWN			
CHK'D			
APPV'D			
MFG			
Q.A			

TITLE:

MATERIAL: Resin

DWG NO. Pulley Ring

A4

WEIGHT: 0.26

SCALE:5:1

SHEET 1 OF 1

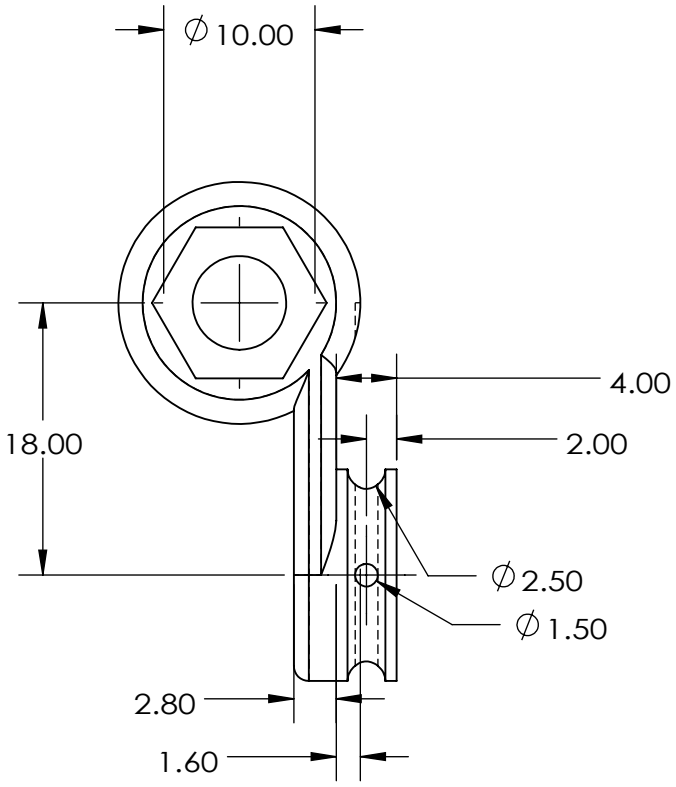

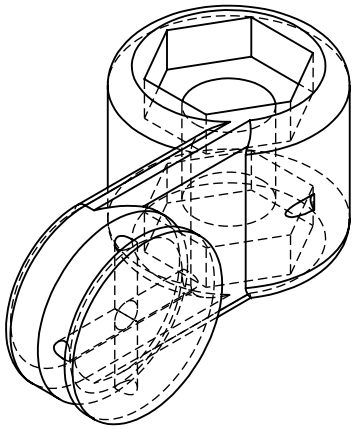

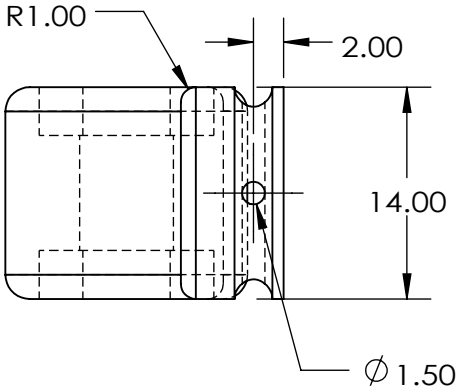

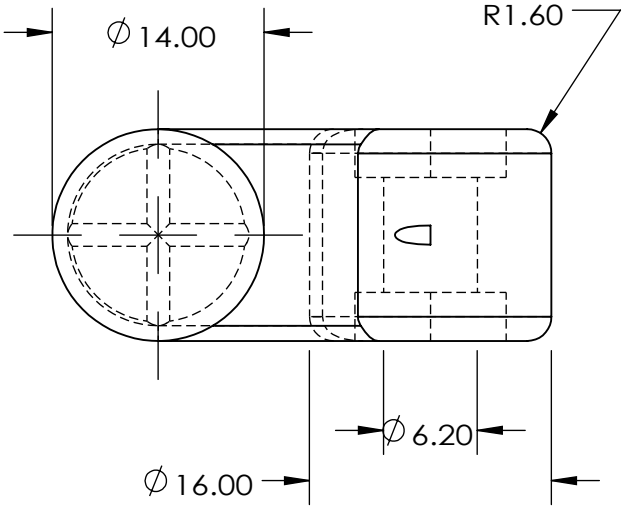

UNLESS OTHERWISE SPECIFIED: DIMENSIONS ARE IN MILLIMETERS SURFACE FINISH: TOLERANCES: LINEAR: ANGULAR:	FINISH: FDM 3D PRINTED	DEBURR AND BREAK SHARP EDGES	DO NOT SCALE DRAWING / REVISION

	NAME	SIGNATURE	DATE
DRAWN			
CHK'D			
APPV'D			
MFG			
Q.A			

TITLE:

MATERIAL: PLA

DWG NO. Slider

A4

WEIGHT: 4.06

SCALE:2:1

SHEET 1 OF 1

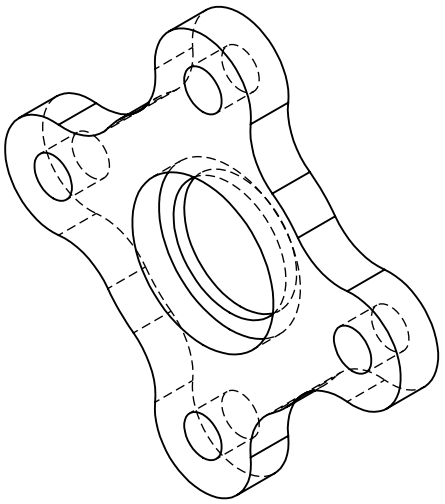

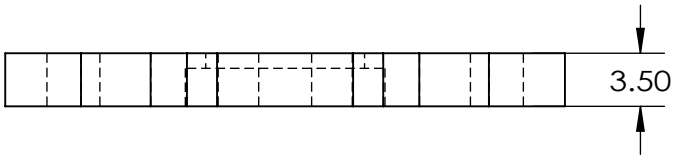

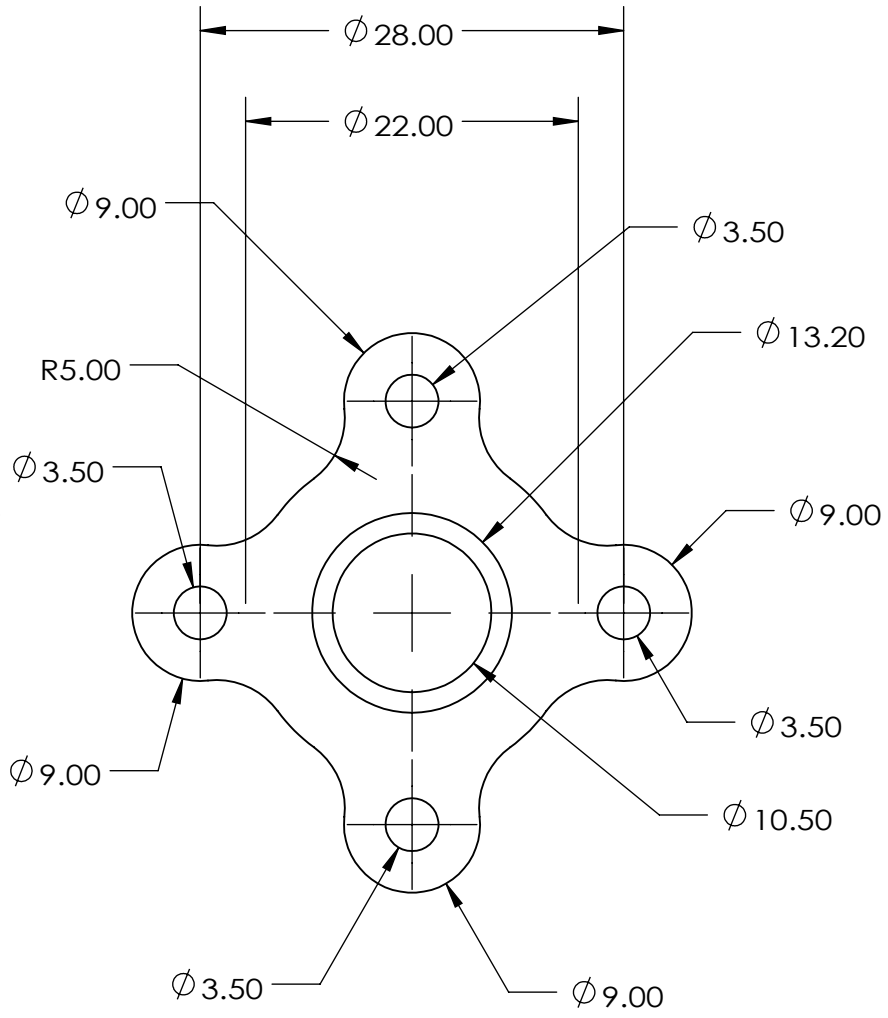

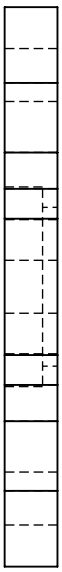

UNLESS OTHERWISE SPECIFIED: DIMENSIONS ARE IN MILLIMETERS SURFACE FINISH: TOLERANCES: LINEAR: ANGULAR:		FINISH: FDM 3D PRINTED		DEBURR AND BREAK SHARP EDGES		DO NOT SCALE DRAWING	REVISION
	NAME	SIGNATURE	DATE				TITLE:
DRAWN							
CHK'D							
APPV'D							
MFG							
Q.A				MATERIAL:		DWG NO.	A4
				PLA		Slider Lid	
				WEIGHT: 2.15		SCALE:2:1	SHEET 1 OF 1

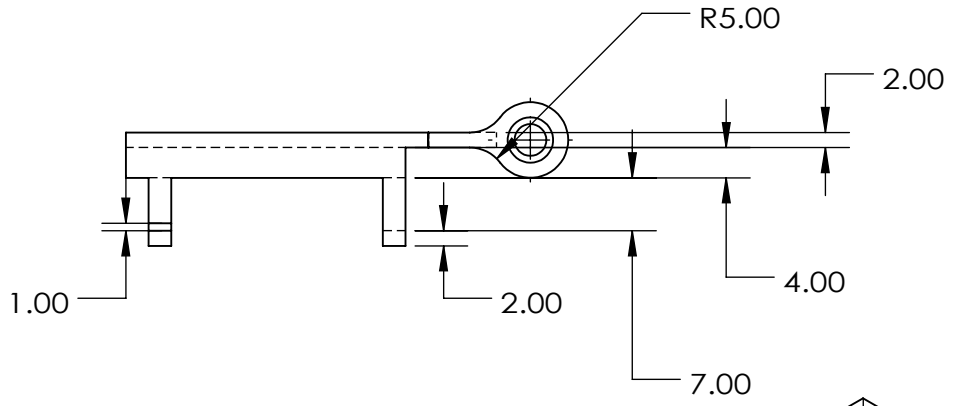

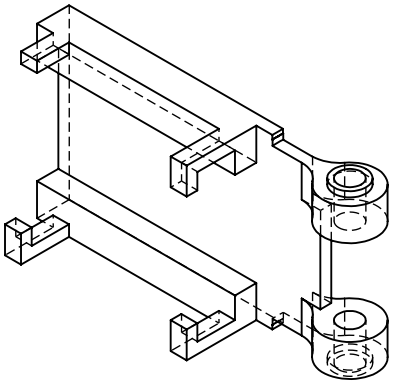

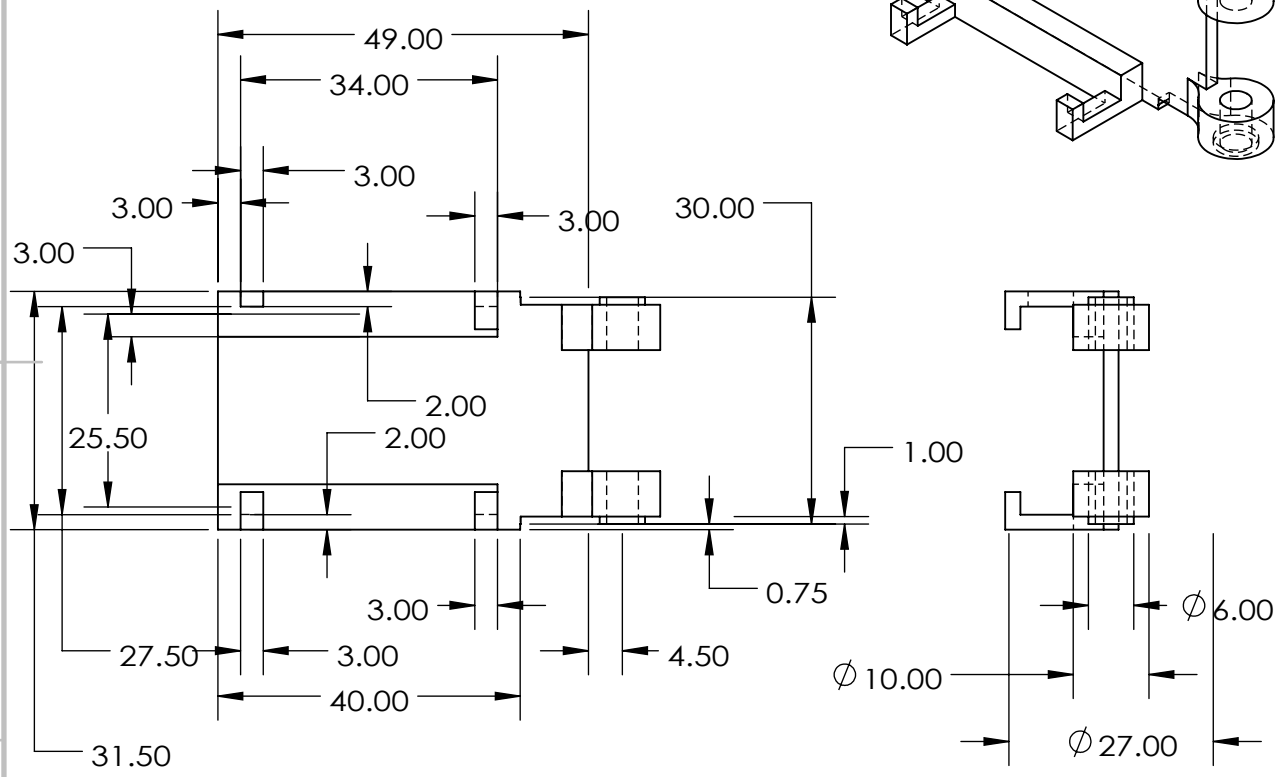

UNLESS OTHERWISE SPECIFIED: DIMENSIONS ARE IN MILLIMETERS SURFACE FINISH: TOLERANCES: LINEAR: ANGULAR:	FINISH: FDM 3D PRINTED	DEBURR AND BREAK SHARP EDGES	DO NOT SCALE DRAWING / REVISION

	NAME	SIGNATURE	DATE
DRAWN			
CHK'D			
APPV'D			
MFG			
Q.A			

TITLE:

MATERIAL: PLA

DWG NO. Friction Plate Holder

A4

WEIGHT:

SCALE:1:1

SHEET 1 OF 1

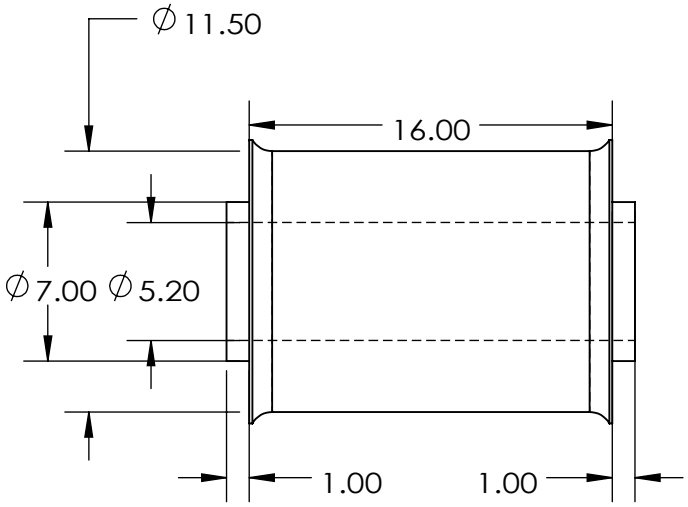

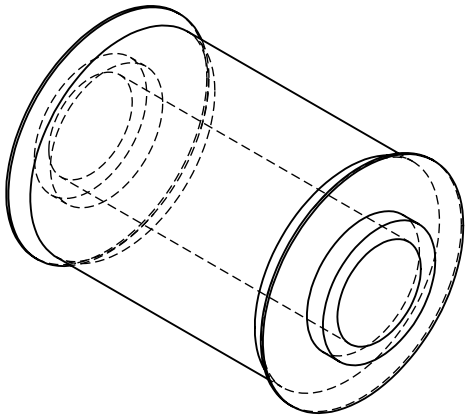

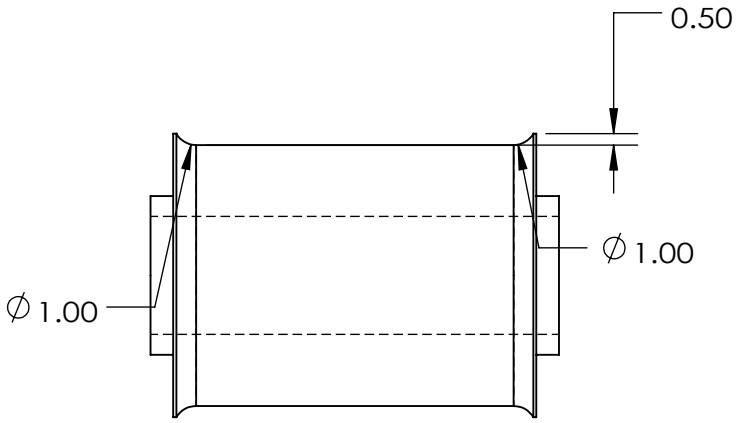

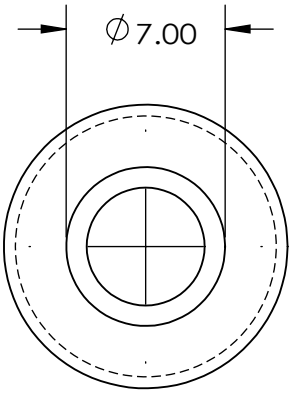

UNLESS OTHERWISE SPECIFIED: DIMENSIONS ARE IN MILLIMETERS SURFACE FINISH: TOLERANCES: LINEAR: ANGULAR:	FINISH: SLA 3D PRINTED	DEBURR AND BREAK SHARP EDGES	DO NOT SCALE DRAWING / REVISION

	NAME	SIGNATURE	DATE
DRAWN			
CHK'D			
APPV'D			
MFG			
Q.A			

TITLE:

MATERIAL: PLA

DWG NO. Translational Pulley Ring

A4

WEIGHT:

SCALE:3:1

SHEET 1 OF 1